IMPACT OF TRIBOSYSTEM COMPATIBILITY ON

TOOL WEAR AND SURFACE INTEGRITY

IMPACT OF TRIBOSYSTEM COMPATIBILITY ON TOOL WEAR AND SURFACE INTEGRITY

By

Taib M. Arif, B.Sc

(King Fahd University of Petroleum's and Minerals, Kingdom of Saudi Arabia)

A Thesis

Submitted to the School of Graduate Studies

in Partial Fulfilment of the Requirements

for the Degree

Master of Applied Science

McMaster University

MASTER OF APPLIED SCIENCE (2015)	McMaster University
(Mechanical Engineering)	Hamilton, Ontario

TITLE:	IMPACT OF TRIBOSYSTEM COMPATIBILITY ON TOOL WEAR AND SURFACE INTEGRITY
AUTHOR:	Taib M. Arif, B.Sc
SUPERVISOR:	Dr. Stephen C. Veldhuis Department of Mechanical Engineering McMaster University
NUMBER OF PAGES:	xi, 101

Abstract

H13 tool steel is widely used in the mold and die industry. Due to tighter geometric tolerances and higher quality expectations, the use of hard machining has increased over the years. Hard machining refers to the machining of materials in their hardened state. The challenges with hard machining are rapid tool wear and maintaining a high surface integrity of the machined surface. Surface integrity is measured in terms of surface roughness, residual stresses, presence of surface and subsurface cracks, and the quality of the developed microstructure. In order to minimize wear and improve product quality, researchers are working on the development of different tool coatings. Some of the recent tool coatings function by adapting to their environment using heat to form thin layers of oxides, referred to as “tribo-films”, on the surface of the tool. If engineered properly, these tribofilms can prolong tool life and improve the surface integrity of a hard machined surface. A titanium based nano multi-layered coating (TiAlCrSiYN/TiAlCrN) has been developed by researchers at the MMRI. The tribological performance of two different coatings TiAlCrSiYN/TiAlCrN and TiAlCrN were tested in a hard machining metal cutting process. The impact of these coatings on tool wear, Cutting process (Chips) and Surface Integrity (Quality of machined surface) was assessed. This research involves characterizing the coating to understand how the formation of different oxide films (tribofilms) effect tool wear and surface integrity. The generation of these tribofilms is sensitive to coating composition and cutting condition (temperature/pressure). Next, an in-depth characterization of the chips produced during machining was carried out as part of studying the effect of different tribological conditions between the tool and workpiece. The chip's hardness, oxidation, chip formation mechanism and topography as the chip slid against the cutting tool surface was studied. Also, the Surface integrity of the machined part was investigated, considering its microstructure, residual stresses and surface roughness. Lastly, tests were performed in an attempt to accelerate the generation of beneficial tribofilms. Results indicate significant improvement in wear life and surface integrity of the machined surface due to the generation of tribo-films in this machining application.

Acknowledgements

I would like to start off by thanking my supervisor, Dr. Stephen C. Veldhuis for giving me the opportunity to study at the MMRI. Dr.Veldhuis has always been very supportive and encouraging throughout my Masters. He has spared no limitations in creating opportunities for me, which has helped me learn, grow and develop into a better individual.

I'd like to thank Dr. German Fox-Rabinovich for his guidance, detailed discussion and sharing of his deep knowledge. I'd like to thank and acknowledge our MMRI team, specially Terry Wagg, Simon Oomen-Hurst, Mohammad Tauhiduzzaman, Julia Dosbaeva and my fellow students for their guidance and help in everyday tasks.

I'm grateful to some of the professors from my undergrad, Dr. B. Yilbus, Dr. S. Zubair, Dr. S. Nouari and Dr. H. Abbas for their motivational talks and guidance everytime I visited Saudi Arabia during the holidays.

Lastly I'd like to acknowledge my mom, dad and baby brother for their endless love, constant support, guidance and prayers. Without them it wouldn't have been possible.

Table of Contents

List of Figures

List of Tables

Chapter 1 Introduction

1.1 Motivation

Improving the productivity of the machining process and the quality of machined parts will allow Canadian companies to be more competitive at a global scale. Through this study, higher quality parts manufactured using extremely high cutting speeds, which have been tuned for high productivity under dry milling conditions, were used. By opting for a dry cutting condition (coolant free), the thermal cycling of the tool is reduced, which is critical for tool life in this case and the cost of using coolant is avoided. Some researchers have speculated that the total cost of using liquid coolant can be as high as 15-20% of the total production cost when the cost of the oil, pumping, its maintenance, disposal, and health and safety issues are considered [Cheng, 2008; Sreejith and Ngoi, 2000]

This study focuses on optimizing the use of a coated tool by prolonging its service life. The tool coating generates tribofilms as a result of interaction with the environment during cutting. These tribofilms are thin layers of oxides which provide the coating with lubricious and thermal barrier properties. By increasing the rate at which these tribofilms are generated, the improvement in tool life and other possible benefits have been explored. Prolonging tool life with controlled output in the form of high quality parts is the goal of all manufacturers. By extensively studying surface integrity, one can understand the role tool coatings and machining parameters have on the quality of the final machined part. Through this research, knowledge can be passed on to local manufacturers who can benefit from it and gain competitive advantages by applying this knowledge in their operations.

1.2 Objectives

The main objectives of this research are the following:

1. To study the importance of coating composition and structure. Illustrating the importance of tribological compatibility for improving tool life and productivity.
2. Studying and illustrating the impact of tribological compatibility on tool wear, the efficiency of the cutting process and on surface integrity of a machined surface at different tool orientations.
3. Studying of chips, which supplement our understanding by giving a full picture of the cutting process and coating performance.
4. Attempt to further enhance tool life by looking into important coating deposition parameters such as argon etching time, and assessing their impact on accelerating the formation of tribofilms which are primary significant mode of protection for advanced coatings.

1.3 Thesis outline

Chapter 1 of this thesis illustrates the motivation and objective behind this research followed by a literature review in chapter 2. Chapter 3 provides details on the experimental setup and procedure. Chapter 4 outlines the main results and provides a discussion on them. Chapter 4 is broken down into 4 subsections. Section 4.1 illustrates the importance of the tribological behaviour of a tool coating. Section 4.2 analyzes chips and the different chip formation mechanisms resulting from the use of different coatings. In section 4.3, the impact these coating have on surface integrity of the machined surface at different tool orientations is studied. Finally, in Section 4.4 the results associated with studies aimed at further enhancing the tribological behaviour of the tool are outlined. Chapter 5 summarizes the findings of this research. Lastly, Chapter 6 provides suggestions for future research in this topic.

Chapter 2 Literature Review

2.1 Metal cutting

2.1.1 High Speed Machining (HSM)

Cutting conditions, especially the cutting speed, are dependent on workpiece material and workpiece material properties. Machining of aluminum at a speed of 1000m/min is considered conventional machining. On the other hand, machining steel alloys and titanium at a speed of 500m/min is considered high speed machining (HSM) [Schulz and Moriwaki, 1992]. To compete globally, manufacturers need to operate their processes at as a high a production speed as possible to allow for a high material removal rate (MRR). In addition, HSM also has been shown to dissipate more of its heat into the chip rather than into the workpiece hence improving surface integrity (SI) [Hirao, et al., 1998; Fallböhmer, et al., 2000]. [El-Wardany, et al., 2000] reported that as much as 80-90% of the heat can be dissipated in the chip with only 10-15% going into the tool and workpiece when using HSM. HSM is commonly used in aerospace, automotive, and mold/die industries [Tlusty, 1993]. It has been reported that the cost associated with machining of a part and its final surface preparation can be as high as 66% of the total cost [Fallböhmer, et al., 1996]. HSM of a part under ideal cutting parameters can decrease this cost by machining a part close to the desired finish in one processing step, hence reducing post machining costs. One of the disadvantages associated with HSM is the severe tool wear that can take place due to the high speeds involved. In addition, HSM requires rigid machine structures and the use of tooling with advanced coatings.

2.1.2 Cutting Tools and Substrate Material

A critical issue associated with machining mold and die materials in their hardened state is the high workpiece hardness and the high temperatures generated during machining. Therefore, there is considerable demand to design cutting tools that last under these harsh conditions. Designing of the substrate material plays an important role, it must be able to support the cutting loads while resisting fatigue and plastic deformation. Some of the common substrate materials found commercially are polycrystalline cubic boron-nitride (CBN), polycrystalline diamond based (PCD) and tungsten carbide (WC) as well as Silicon Nitride (SiN) and Aluminum Oxide (AlO) ceramic materials. Table 2-1 illustrates some of the properties of these cutting tool materials.

Table 2-1: properties of cutting tool material (Fallböhmer, et al. 1996)

	Tool material				
	PCD	CBN	WC	SiN	AlO
Micro-Hardness (HV)	6000	3500	1500-1800	1700	1600
Thermal Conductivity (W/m K)	500	100	40-80	15-35	14-17

CBN based substrates are extremely hard and are resistant to diffusion making them applicable for high speed machining. It was found that CBN performed extremely well in machining of P20 mold steel at cutting speeds as high as 1000m/min. Compared to machining with tungsten carbide substrates, alumina used as the binder in the CBN tools minimized diffusion wear giving almost double the tool life [Movahhedy et al., 2000; Ren &Altintas, 2000].

Tungsten carbide (WC)

Tungsten carbides are generally cheaper than CBN tools and are preferred for mass production. The grade of the tungsten carbide tool is dependent on three factors: the chemical composition of the binder, grain size of the carbide particles, and their hardness. Carbide tools which possess high abrasion resistance with fine grained uniform microstructure are required in high speed machining. In milling, since the nature of cutting is interrupted with cyclic loading, not only does the tool need to be hard, it also needs to acquire high toughness. One of the elements that plays a crucial role in determining WC's properties is the percentage of cobalt binder used to hold the fine grains of WC together to form the tool. Cobalt can range from 5-12 wt % in cutting tools. Table 2-2 provides a quick guide to the characteristics of a tungsten carbide cutting tool. Due to the high cutting temperature in the cutting zone, there is a decrease in fracture strength when operating at a temperature in excess of 500°C. For WC tools, the decline in strength is associated with the surfaces oxidation rate [Acchar et al., 1999; Tlusty& Masood, 1978], which serves to define the limiting cutting speed in many applications.

Table 2-2: Quick guide to characteristics of tungsten carbide [Electronic Machine tools Ltd., 2007; Elfizy, 2008]

		Impact on following properties:				
		Cobalt%	Abrasion Resistance	Grain Size	Hardness	Fracture Toughness
When you increase	Cobalt%		↓		↓	↑
	Abrasion Resistance	↓		↓	↑	↓
	Grain Size		↓		↓	↑
	Hardness	↓	↑	↓		↓
	Fracture Toughness	↑	↓	↑	↓	

2.1.3 Types of Tool Wear and Tool Wear Mechanism

[Yen et al., 2002] has classified the reasons of tool wear into 4 groups. Firstly the properties (mechanical and thermal) of how workpiece material affects the temperature, forces, and wear. Secondly, the tribology at the tool chip interface and its effect on tool wear mechanisms and cutting processes. Thirdly the cutting tool itself, its chemical properties and geometry and their influence on tool wear. Lastly, the machine tool system, its dynamics and stability and how they influence the cutting process and tool wear.

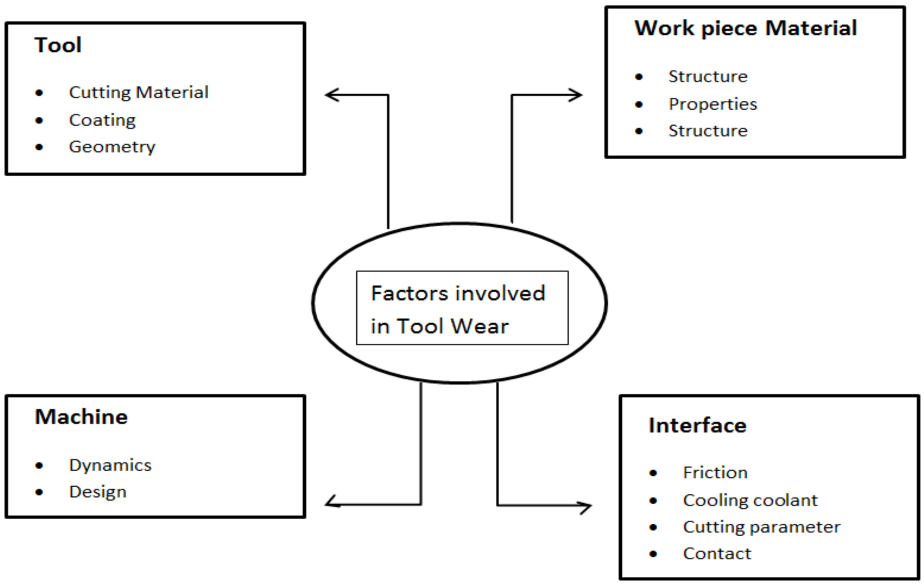

Figure 2-1: Factors influencing tool wear [Based on Yen, et al., 2002]

Types of Tool Wear

The following types of tool wear are seen on cutting tools:

Flank wear is the flat land that forms on the flank face. It is one of the most commonly found tool wear patterns and it occurs due to abrasive wear mechanisms. An increase in flank wear can lead to poor surface integrity and dimensional accuracy. ISO 3685:1993 and ISO 8688-2:1989 describe tool life testing techniques for turning and milling respectively and set a reasonable tool life criterion to be 0.3mm of flank wear.

Crater wear occurs on the rake face of the cutting tool. It forms due to the sticking and sliding motion of the chips along the rake face at high temperature and stress. Crater wear is formed due to abrasion, diffusion and adhesion wear mechanisms. Crater wear can lead to catastrophic breakage of the cutting edge as the support for the cutting edge is eroded away.

Notch wear is a notch that forms on the flank face and is often associated with the depth of cut. This wear occurs due to oxidation as well as the presence or formation of hard particles on the surface layer of the tool and due to chips hitting the edge forming a notch.

Build up edge (BUE) occurs when the workpiece material adheres onto the cutting edge changing the tool edge geometry. Layers upon layers of workpiece material stick and weld on to the tool edge until reaching a critical size after which it breaks off catastrophically, often taking a piece of tool material with it.

Thermal and mechanical fatigue wear is caused by cyclic loads. These cyclic loads can be thermal as well as mechanical in nature. In interrupted cutting such as milling, the cutting edge is constantly engaging and disengaging. During the cut, the cutting edge gets heated, and upon disengagement, the tool is rapidly quenched by coolant or air when dry machining. Due to thermal shock, cracks initiate which are perpendicular to the cutting edge. Similarly the cutting edge experiences fluctuating mechanical loads which initiate cracks that are parallel to the cutting edge.

Chipping occurs when the tool is brittle and is not strong enough to handle the cyclic loads.

Plastic deformation occurs when the cutting edge experiences high stresses and temperatures which are in excess of the yield point causing the tool edge to plastically deform.

Tool Wear Mechanisms

Mechanisms associated with tool wear are due to high cutting temperatures, high normal and shear stresses, and presence of cutting fluid if coolant is being used. Figure 2-2 illustrates the different wear mechanisms involved in metal cutting. Figure 2-3 illustrates the correlation of these wear mechanisms at different cutting speeds.

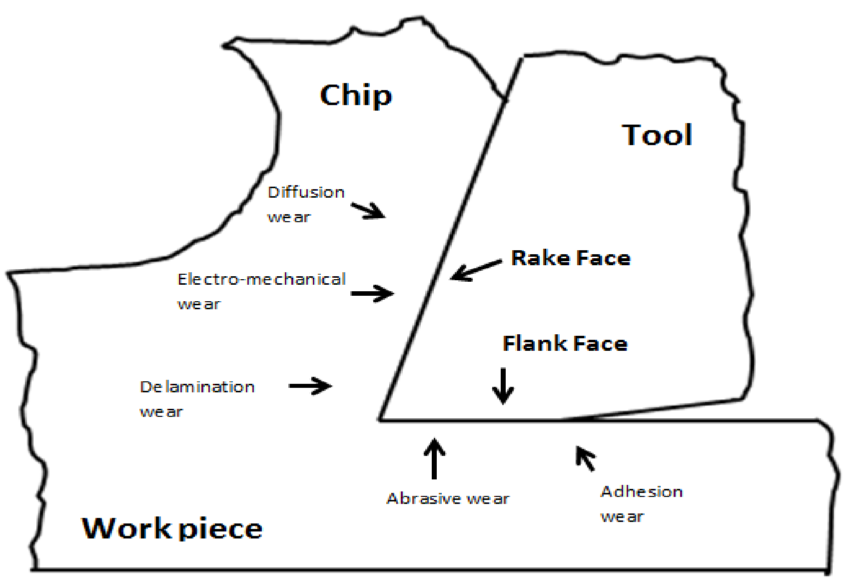

Figure 2-2: Wear mechanisms in cutting [Based on Kopac, et al. 2001]

Abrasive wear is when hard particles from one surface scratch and remove materials from another surface which is softer. In machining the workpiece materials are often heat treated and in some cases have hard particles like carbides or silicon oxide present in their structure. These hard particles can scratch the tool's surface when the chip slides along the rake face and flank face, causing the tool to wear.

Adhesive wear is when workpiece material adheres and sticks on to the tool's surfaces. Due to high temperature and pressure workpiece material can adhere to the tool and often times the working of the material during cutting tends to harden it. When shear stress is applied the adhered material gets removed, taking some of the tool material with it.

Diffusion wear occurs when an element from the tool diffuses in to the workpiece materials causing the tool to weaken and break. The diffusion rate is dependent on tool/workpiece material compatibility, cutting temperature, and concentration gradient. Diffusion/chemical wear is mostly seen on the rake face [Braghini and Coelho, 2001].

Oxidation wear occurs when metals are exposed to oxygen at high temperature/pressure. In cutting tools it is seen as a large notch.

Fatigue wear can be broken into two categories: mechanical fatigue, and thermal fatigue. Mechanical fatigue occurs due to cyclic compressive and tensile stresses, whereas thermal fatigue occurs due to cyclic heating and cooling. These cyclic loads initiate micro cracks which lead to chipping over time. In milling we see both mechanical and thermal fatigue. As a tooth engages into cut it experiences high compressive stresses which are released when the tooth disengages. The same tooth when cutting is heated, which experiences thermal shock when it disengages and is flooded with coolant.

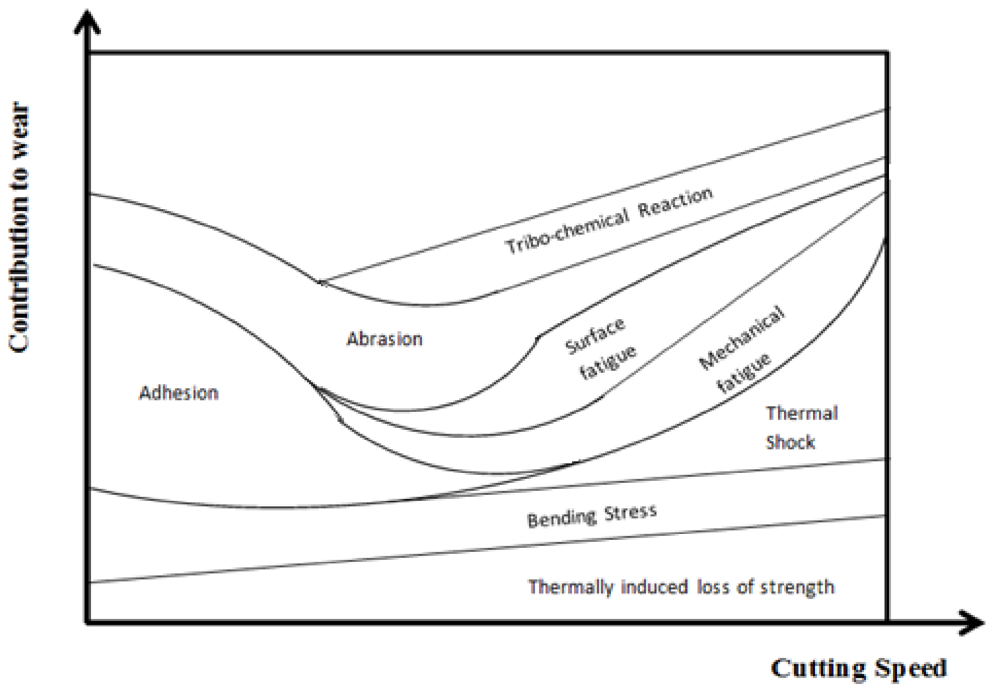

Figure 2-3: Correlation between different tool wear mechanism and cutting speed for interrupted cutting [Based on Löeffler, 1994]

2.2 Coating

2.2.1 Needs for Coating and Coating Techniques

Heat in metal cutting is generated primarily from three zones. Firstly, the primary shear zone where the material shears and plastically deforms at a very high strain rate, generating large amounts of heat. Next the secondary shear zone where the chip's sliding motion along the rake face generates heat due to friction, and lastly the tertiary shear zone where heat is generated due to the rubbing of the flank face of the tool against the machined surface. These three zones are referred to as the cutting zone or the contact zone. In milling, the cutting operation is interrupted in nature, and hence worsening the condition with mechanical as well as thermal fatigue. The heat that is generated during cutting is dissipated into the (i) tool, (ii) chip and (iii) workpiece. Due to the surface interactions it is important to consider the role that a coating can have on the level of heat that is being generated and how heat is redirected for the given three bodies. Figure 2-4 illustrates the possible impact that a coating can have in a cutting process. Therefore it is important to design a coating that withstands the harsh cutting conditions and provides wear resistance and lubricity and serves as a thermal barrier.

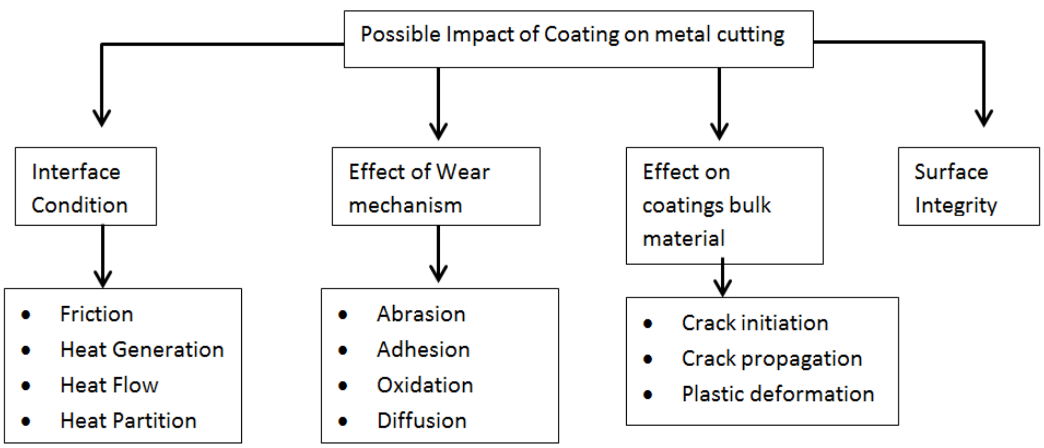

Figure 2-4: Possible impact of coating during cutting [Based on Grzesik and Nieslony, 2003]

Coatings consist of three zones. The first zone is the coating bulk material, where the coating composition and microstructure determine the coating properties. The second zone is the interface between the coating and substrate. Here, adhesion of the coating along with chemical and physical compatibility of the coating with the substrate material, such as its thermal coefficient of expansion, is important. The third zone is the top or outer layer of the coating. Designing this layer impacts how it will interact with the workpiece and ultimately the surrounding environment. For a coating to be successful all of these three zones have to be studied and the coating must be designed to sustain the local operating conditions of high load and temperature. Figure 2-5 illustrates the requirements and influences of the coating and substrate.

The two most common techniques for coating deposition are Chemical Vapor Deposition (CVD) and Physical Vapor Deposition (PVD). Typically for interrupted cutting tools, PVD coating is preferred as it allows maintaining the sharpness of the cutting edge with minimal rounding. In addition, the PVD coating process doesn't lead to the same level of substrate embrittlement as can occur with CVD processes. The PVD process is also quite flexible with regards to coating composition. Lastly, compared to CVD, PVD coating usually gives desirable residual stresses on the coating surface [Ning, 2007]. PVD coating is performed in a vacuum chamber with a target material as a vapour source. A medium is required such as Argon based plasma to deposit the target material onto the part. PVD techniques widely used for deposition of Ti-Al based coatings are cathodic arc [Suzuki, et al., 1998], magnetron sputtering [Kukla, 1997] and a hybrid system which combines cathodic arc with magnetron sputtering [Yamamoto et al., 2005]. These techniques differ in how the target material is evaporated. During deposition, reactive gas such as nitrogen is introduced which reacts with the metal vapor making it thin and adherent [Ning, 2007]. The tools in the coating chamber are constantly rotating to ensure uniform coating deposition. Rotation past different targets allows for the layering of different materials to form a coating.

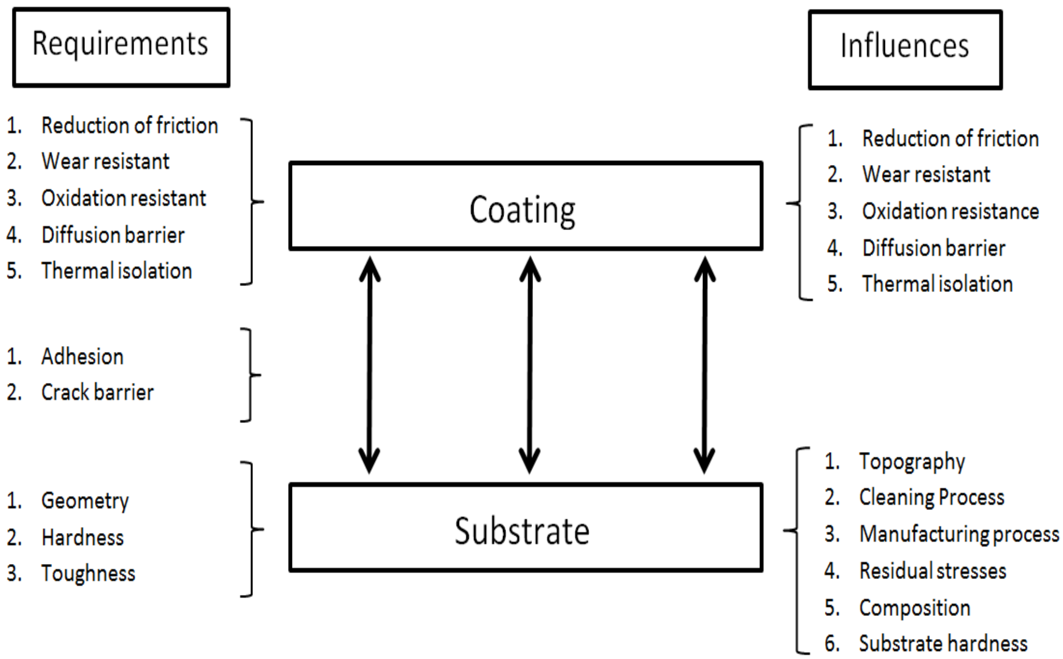

Figure 2-5: Requirements and Influences of coating and substrate [Based on Tönshoff, et al., 2002]

2.2.2 Coating Material Selection and Effect of Alloying Elements

For specific purposes, it is important to select the right materials for coating composition. Hard PVD coatings commonly contain transition metals such as Titanium, Zirconium etc., which are used for their properties such as high tensile strength, high density, melting and boiling points [Ning, 2007]. Metallic, ionic and covalent bonds are typically the three bonds commonly found in hard coatings [Holleck and Schier, 1995]. Table 2-3 illustrates examples of the bonds found in some of the coatings.

Table 2-3: Examples of bonds [Holleck and Schier, 1995].

Type of bond	Example
Metallic	Nitrides of Ti
Covalent	Nitrides of Al and Si
Ionic	Oxides of Al,Ti

Generally, for high speed dry machining, where cutting temperatures are extremely high (1000ºC) and pressure can be as high as 3-5 GPa, TiAlN based coatings are preferred. For a coating to operate in such severe conditions, high levels of hardness are required at high temperatures. Higher hardness results in lower abrasive wear. Coatings have a tendency of losing its hardness at elevated temperature. Loss of hot hardness is a possible indication that the coating has had a high residual stress at room temperature. Ideally we would want a coating to have high hardness and low residual stress, since high residual stress can cause poor adhesion to the substrate [Paldeyand Deevi, 2003].

There are two temperatures associated with oxidation: the temperature at which oxidation is initiated, and the temperature at which rapid oxidation occurs. If rapid oxidation occurs, the tool rapidly fails. However, some level of oxidation has been shown to be beneficial [Fox-Rabinovich et al., 2012]. Ideally, one would prefer the tool operating within these two temperature limits. Both hardness and oxidation can be further enhanced by adding alloying elements. Table 2-4 illustrates the effect of using different alloying elements in the coating matrix.

Table 2-4: Effect of alloying elements on coating property

Alloying Element	Effect on property of coating and during cutting
Aluminum	• Increases hardness and hot hardness [Paldey and Deevi, 2003] • Generation of Aluminum based oxides during cutting [Fox-Rabinovich et al., 2012]
Yttrium	• Improves oxidation and corrosion resistance [Smith, et al., 1997] • Causes grain refinement [Ning, 2007] • Helps delay rapid oxidation temperature [Paldey and Deevi, 2003]
Chromium	• Improves oxidation and corrosion resistance [Smith, et al., 1997] • Formation of Chromium oxide (Cr-O), which acts as a lubricant [Fox-Rabinovich, et al., 2005]
Silicon	• Increases hardness in Titanium aluminum based coating [Ning, 2007] • Helps improve oxidation resistance and thermal stability [Ning, 2007] • Helps in formation of Mullite [Fox-Rabinovich et al., 2012].

2.2.3 Effect of Grain size

Conventional grain size materials are ones where the grain size is 0.1μm, as shown in Figure 2-6. Nano materials are materials which possess grain size lower than 100nm. According to the Hall-Petch relationship, $H(d) = H_o + Kd^{-0.5}$ (d is the grain size), the hardness of the material increases as the grain size decreases, approximately up to 10nm. A further reduction in grain size results in a decrease of hardness [Zhang, et al., 2003]. Prior to 10nm, the mobility of dislocations is hindered, however below 10nm, a decrease in the hardness of the coating is observed and is attributed to grain boundary sliding.

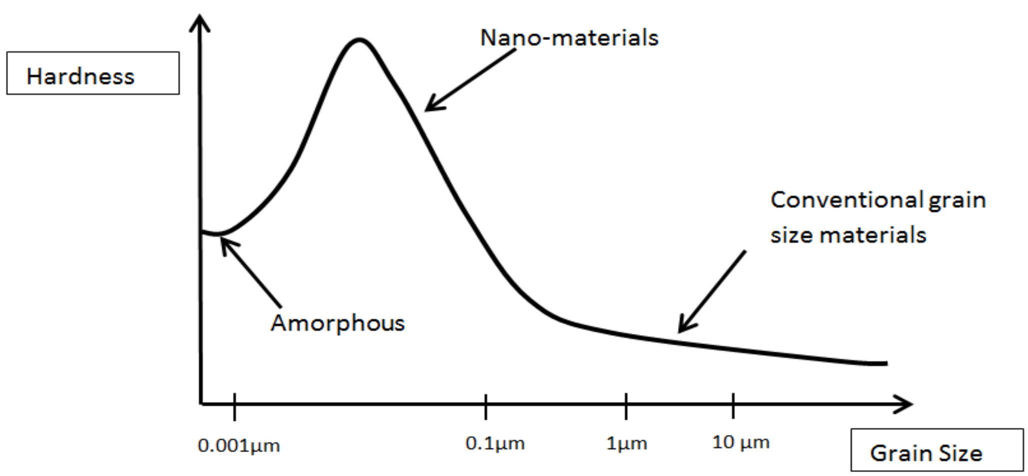

Figure 2-6: Effect of grain size on material hardness [Based on Zhang, et al., 2003]

2.2.4 Effect of coating structure

Hard PVD coatings can be characterized primarily into seven groups, Multi-component coating, Super-lattice coating, Dispersion coating, multiple layer coating, Nano structured coating, Self-lubricating coating and Self-adaptive coating [Jehn, 2000; Fox-Rabinovich, et al., 2006]. The two most common coatings found for machining of H13 tool steel at high speeds, are Multi component coatings and self-adaptive coatings. Examples of these two are given in Table 2-5.

Multi component coatings started with TiN, which is a binary multi component coating. Later, different alloying elements were added to improve the properties. [Knotek et al., 1987] reported a ternary multi-component coating of TiAlN which resulted in improved properties. A quaternary multi-component coating designed with addition of the elements Yttrium [Donohue, et al., 1997], and Chromium [Lewis, et al. 1999, Fox-Rabinovich, et al., 2006] were reported.

Self-adaptive coatings can respond to external stimulus and have been observed to adapt to their conditions. In cutting, these external stimuli can be in the form of heat and pressure [Fox-Rabinovich, et al., 2006]. It has been observed that these coatings respond by forming thin layers of oxides also referred to as tribofilms. These tribofilms can serve as thermal barriers and provide lubricious properties. Properties of these tribofilms are dependent on the coating composition and cutting parameters.

Designing these coatings in multilayers can lead to further enhancement in machining performance. Coatings consisting of alternating layers of different coatings have shown a reduction in grain growth [Ning, 2007]. Multi-layer coatings increase the number of interfaces, which helps in deflecting the direction of grain growth along the interface, rather than into the coating [Holleck and Schier, 1995]. Multi-layer coatings have also been shown to decrease the delamination size of the coating from large scale delamination to fine scale delamination [PalDey and Devvi, 2003].

Table 2-5: Coating Structure and Examples

Coating Structures	**Example**
Multi-component coating	TiN, (Ti,Al)N, (Ti,Al,Cr)N
Self-Adaptive Coating	TiAlCrSiYN/TiAlCrN

2.3 Surface Integrity

2.3.1 Introduction

The concept of surface integrity (SI) is defined as "the inherent or enhanced condition of the surface produced after machining or any other surface generation process" [Astakhov, 2010; M'Saoubi, 2008; Field and Kahles, 1964]. The generated surface can have altered characteristics or properties during machining. The altered layer may be very small and localized only at the surface of the workpiece with its resulting performance in subsequent activities greatly affected. Surface alteration may result in surface topography, surface metallurgy, chemical and mechanical property changes which effect its resistance to wear, fatigue, corrosion, adhesion and diffusion [Astakhov, 2010].

Layers in Manufactured Surface

A surface is the outer most layer of any object. There can be a presence of a transition layer from the surface to the bulk which exists when there is a change of chemical and physical properties such as density and crystal structure [Hudson, 1992]. Though the performance of a component is primarily determined by the bulk property, surface properties play a crucial role in wear resistant components since wear initiates at the surface. Surfaces generated during machining are not smooth at the microscopic scale and can be considered very rough at the atomic scale. For metals, these surfaces tend to oxidize even at room temperature. The diffusion of atoms from the workpiece and surrounding determine the oxidation rate. In machining, the surface undergoes severe plastic deformation forming a deformation layer. The oxidized particles are embedded into the surface and covered with moved material. This forms a layer which is a mixture of metal and oxide. Figure 2-7 illustrates different layers present on the surface of a manufactured component. Depending on the manufacturing process, there is the presence of a worked layer which can range from 1-100 μm in thickness. On top of it is a layer referred to as the Beilby layer. The Beilby layer can be amorphous, nano- or micro-crystalline and is formed due to the melting of the material and its surface flow during machining [Finch, Quarrell and Roebuck, 1934]. Next is an oxide layer which is formed due to the presence of oxygen in the environment, and surface oxidation mechanisms. Finally, a layer of adsorbent material which consists of water vapour and hydrocarbons, which might have condensed onto the surface from the environment.

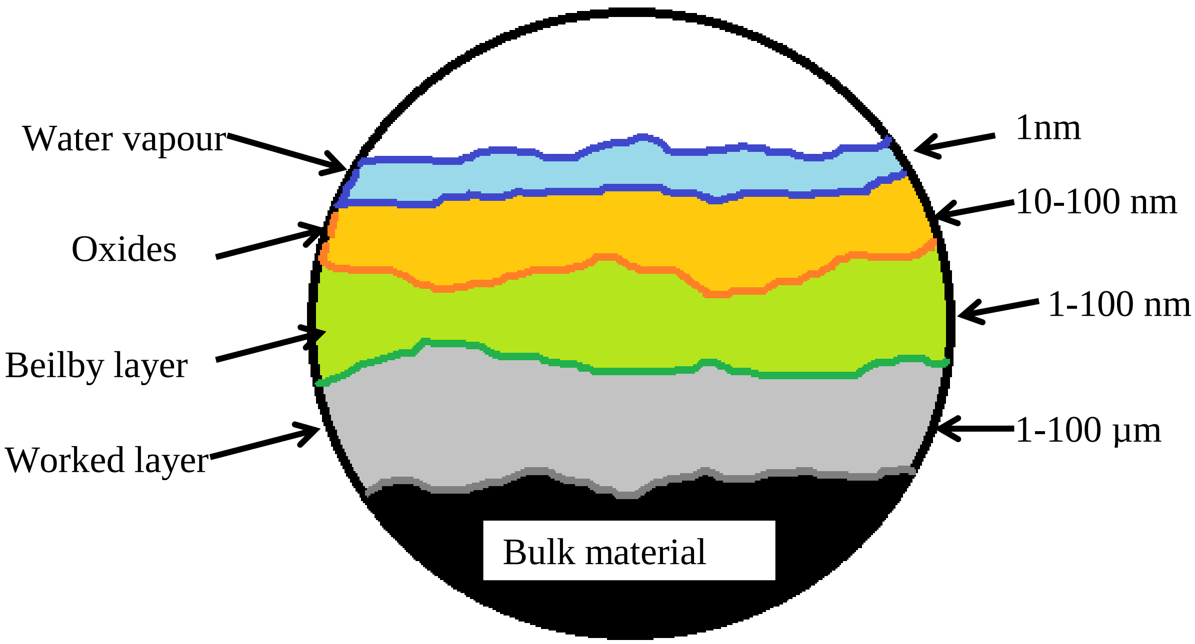

Figure 2-7: Schematic of a manufactured surface [Based on Astakhov, 2010]

Defects on manufactured surfaces

Defects in manufacturing can be classified into two categories: a defect in the original material which is now exposed or defects caused by the manufacturing process. Common defects found during manufacturing are cracks, voids, metallurgical transformations caused by temperature and pressure as well as residual stresses, and inclusions.

Severe plastic deformation occurs during machining causing cold working of the surface. Cold working of the surface results in an increase of hardness and tensile strength whilst lowering ductility and impact value [Astakhov, 2010]. When in its hardened state there is involvement of rapid thermal processes which causes a metallurgical transformation. According to [Chou and Evans, 1999] the worked surface is composed of three aspects; white layer, metallurgical change, and residual stress. This can result in a difference in structure as compared to the bulk material. One of the major factors determining surface properties is the flank wear on the tool. The flank of the tool rubs against the workpiece affecting the surface integrity, hence a tool life criteria based on flank wear is particularly relevant in this case.

2.3.2 Surface Finish

Micro and Macro Surface Deviation

The term surface finish helps define a physical quantity to the quality of a manufactured surface. Surfaces machined as prescribed in drawings with no consideration of irregularities are referred to as the nominal surface. A real surface profile takes into account the surface details at the microscopic level. The surface is measure using mechanical or optical devices. Usually these measurements are taken in a direction perpendicular to the cutting feed direction. Most of the asperities are exhibited in this direction, compared to measuring in any other direction. Surfaces irregularities can be broken down into six orders (six categories) as illustrated in Table 2-6. The first two orders are macro-geometric and are associated with form errors and waviness. The remaining four orders are micro-geometric and classified under surface roughness.

Table 2-6: Geometric deviation of machined surfaces [Based on Petropoulos, Pandazaras and Davim, 2010

<table>
<tr><th></th><th>Order</th><th>Deviation</th><th>Causes</th></tr>
<tr><td rowspan="2">Macro-geometric deviation (Errors and waviness)</td><td>1st</td><td>Form errors</td><td>• Errors of machine tool slides
• faulty fixation of tool or work-piece</td></tr>
<tr><td>2nd</td><td>Waviness</td><td>• Eccentric rotation of tool
• Manufacturing system dynamics
• Tool wear</td></tr>
<tr><td rowspan="4">Micro-geometric deviation (Surface Roughness)</td><td>3rd</td><td>Grooves</td><td>• Tool edge form
• Process kinetics
• Chip morphology</td></tr>
<tr><td>4th</td><td>Cracks</td><td>• Tool nose wear
• Built up edge (BUE)
• Chip formation mechanism</td></tr>
<tr><td>5th</td><td>Crystalline structure</td><td>• Chemical reaction
• Corrosive damage</td></tr>
<tr><td>6th</td><td>Crystalline formation</td><td>• Physical and chemical alteration in material structure and lattice</td></tr>
</table>

Measuring parameters

Surface roughness is a micro-geometric deviation. Some of the most common parameters used for measuring surface roughness are R_a, R_t, R_z, R_q (RMS) and R_p. R_a is the most commonly used parameter with "a" standing for average. This method of describing roughness represents the average value of the roughness profile about the centre line over a certain sampling length. It is one of the easiest parameters to define and is very commonly used in engineering drawings. However, it has been shown to be of limited value at detecting surface roughness variation due to small vibrations. R_t is the maximum peak to valley distance over a certain length. It is very sensitive to large deviations (scratches) and can give a wrong interpretation of the surface profile when a few large scratches are present on the surface. R_z is similar to R_t, however it averages the readings of maximum peaks to valleys over a certain length. R_q or RMS is the root mean square of the roughness profile. R_p is the value of the highest peak from the mean line (center line) [Petropoulos, Pandazaras and Davim, 2010].

Figure 2-8 illustrates the different parameters based on a surface profile and their numerical representation. Some of the common factors effecting surface roughness in machining are the cutting conditions, tool wear, dynamics of the machine tool system and mechanical properties of the workpiece material.

	Equation representation	**Graphical representation**
R_a or **CLA** (Centre Line Average)	$R_a = \frac{1}{L}\int_0^L \lvert z \rvert \ dx$	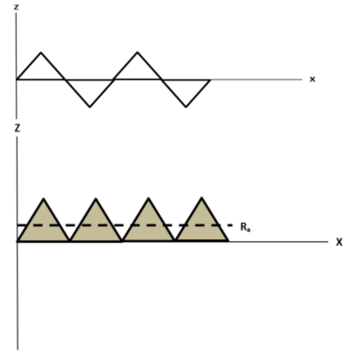
R_q or **RMS** (Root Mean Square)	$R_q = \sqrt{\frac{1}{L}\int_0^L Z^2 \ dx}$	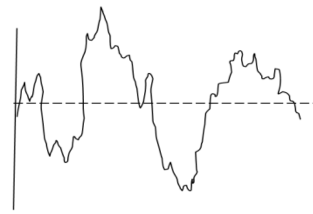
R_t, Maximum Peak to vally	$R_t = \frac{1}{5}\sum_{i=1}^{5} R_{max_i}$	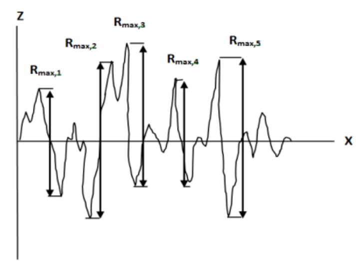
R_z, Ten point height	$R_z = \frac{\sum_{i=1}^{5} \lvert P_i \rvert + \sum_{i=1}^{5} \lvert V_i \rvert}{5}$	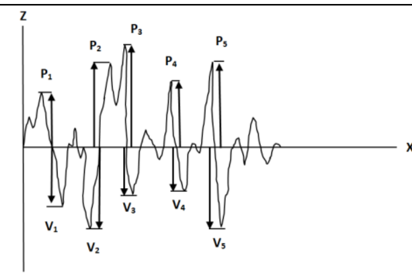
R_p, Maximum peak height	$R_p = \max_i(P_i)$	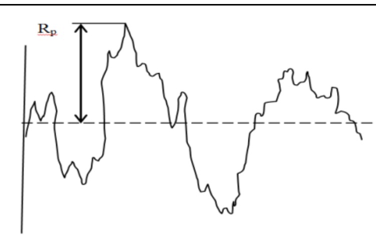

Figure 2-8: Surface roughness parameters [Stachowiak and Batchelor, 2013]

Surface waviness is a macro-geometric deviation as illustrated in Figure 2-9 and it is an indication that the machine tool system is undergoing severe vibration. Similar to measuring surface roughness, there are functional parameters used to measure surface profile in terms of surface waviness. W_a is the mean waviness of the unfiltered profile. W_t is the maximum value of the waviness of the unfiltered profile. W_q represents the RMS deviation (waviness) of the profile. W_p gives the maximum waviness peak height. W_v is the maximum waviness valley depth and Wz represents the maximum height of the assessed profile [Petropoulos, Pandazaras and Davim, 2010]. Mathematical representations of the surface waviness parameter are illustrated in Table 2-7. When studying the surface profile, the scanned data can be filtered and broken down into high and low frequency data. “High pass” filters allow high frequency data to pass through, hence removing waviness. “Low pass” filters allow low frequency data to pass through, hence removing roughness.

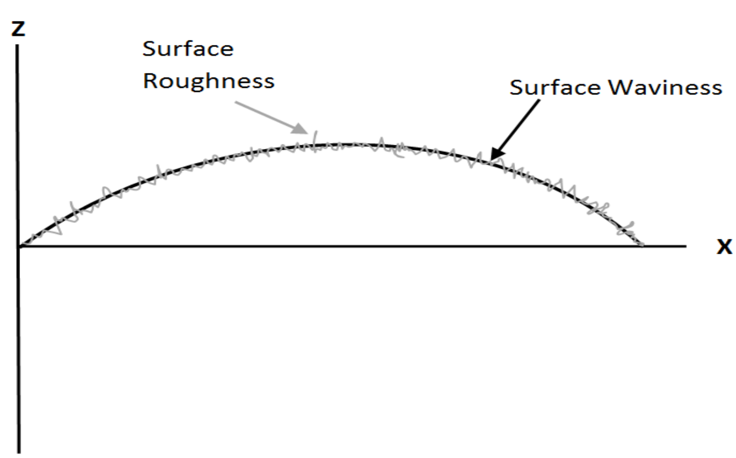

Figure 2-9: Surface Waviness

Table 2-7: Surface Waviness parameters [ISO 4287:1997; ISO 4288:1996]

Waviness Parameter	Equation representation
W_a, Arithmetic mean deviation	$W_a = \frac{1}{n}\sum_{i=1}^{n} \lvert z_i \rvert$
W_q, RMS deviation of the profile	$W_q = \sqrt{\frac{1}{n}\sum_{i=1}^{n} z_i^2}$
W_p, Maximum waviness peak height	$W_p = \max_i(P_i)$
W_v, Maximum waviness valley depth	$W_v = \max_i(V_i)$
Wz, Maximum height of the assessed profile	$W_z = W_p + W_v$

2.3.3 White layer

One of the layers most commonly seen in a machined surface microstructure is referred to as a “white layer”. One of the earliest mentions of white layer was in 1912 by Stead [Stead, 1912] in his work on steel wire ropes. The term “white layer” refers to a featureless white layer which can be observed under an optical microscope and SEM [Griffiths, 1993]. A white layer is also referred to as a white etching layer or white phase [Bosheh and Mativenga, 2006]. The formation of a white layer can be associated with factors such as strain rate, cooling rate, heating rate and the environmental condition [Astakhov, 2010]. A white layer is categorized into two groups with the help of a special etchant [Klocke and Kratz, 2005]. Firstly, it’s the white layer which composes of an austenite phase (over 60%) and remains white compared to dark over tempered martensite even after using a special etchant. The second group of white layer shows a fine grained martensitic structure with the help of a special etchant [Klocke and Kratz, 2005]. Both of these white layers are characterized as defects. Both are highly brittle and prone to cracking. Figure 2-10 illustrates a white layer on the surface of a H13 sample using an SEM after performing dry machining.

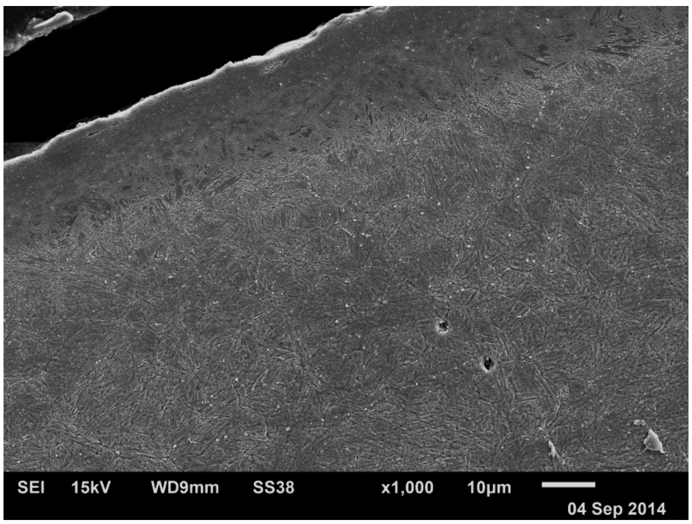

Figure 2-10: White layer formed when machining H13

2.3.4 Effect of cutting edge radius

In metal cutting there are three deformation zones, primary, secondary and tertiary. The tertiary (shear) deformation zone is located below the cutting edge and is related to the subsurface layer. Figure 2-11 illustrates the effect of cutting edge on the distribution of elastic stresses in the subsurface. It can be seen that having a rounded cutting edge expands the compression zone. The material is being plowed and there is a shift to a larger negative rake angle which results in a work hardening effect. It has been reported that an increase of the cutting edge radius increases the hardness [Kaczmarek, 1976].

Rounded Cutting Edge	Sharp Cutting Edge

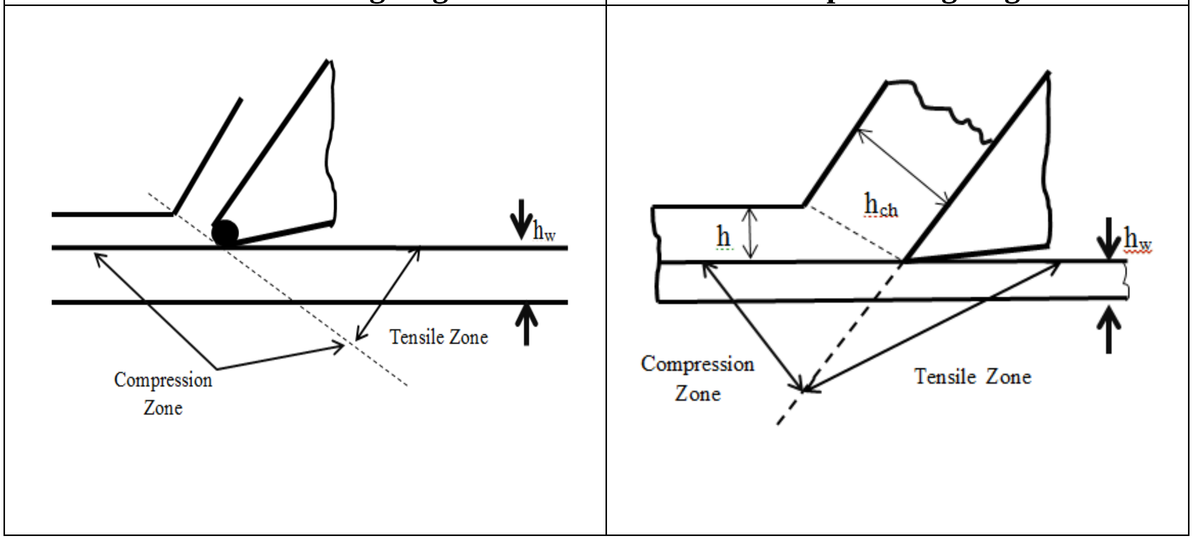

Figure 2-11: Effect of cutting Edge (Grzesik, 2008; Kaczmarek, 1976)

2.3.5 Models for residual stresses

Residual stresses in machining are stresses left on the machined surface. These stresses can be compressive or tensile. Generally for machining of components which are subjected to stresses, it is favourable to have compressive stress. Compressive stress on a surface resists crack propagation. Figure 2-12 illustrates the mechanisms behind the generation of these stresses (Grzesik, 2008).

The first model is the “thermal phase transformation mechanism”. Here, the main mechanism for residual stress is due to an applied heat source which causes the surface material to change its phase. A phase change results in a change in volume. If the phase shift is such that the volume decreases upon cooling, it will result in tensile residual stress. However, an increase in volume can result in a compressive stress. The second model is the “thermal and plastic deformation”. In this model, the applied heat causes the surface layer to expand and plastically deform. Upon cooling, it leaves the surface with tensile stresses. The third model is the “mechanical” model. Here the surface undergoes mechanical action compacting the surface. This usually results in compressive stresses.

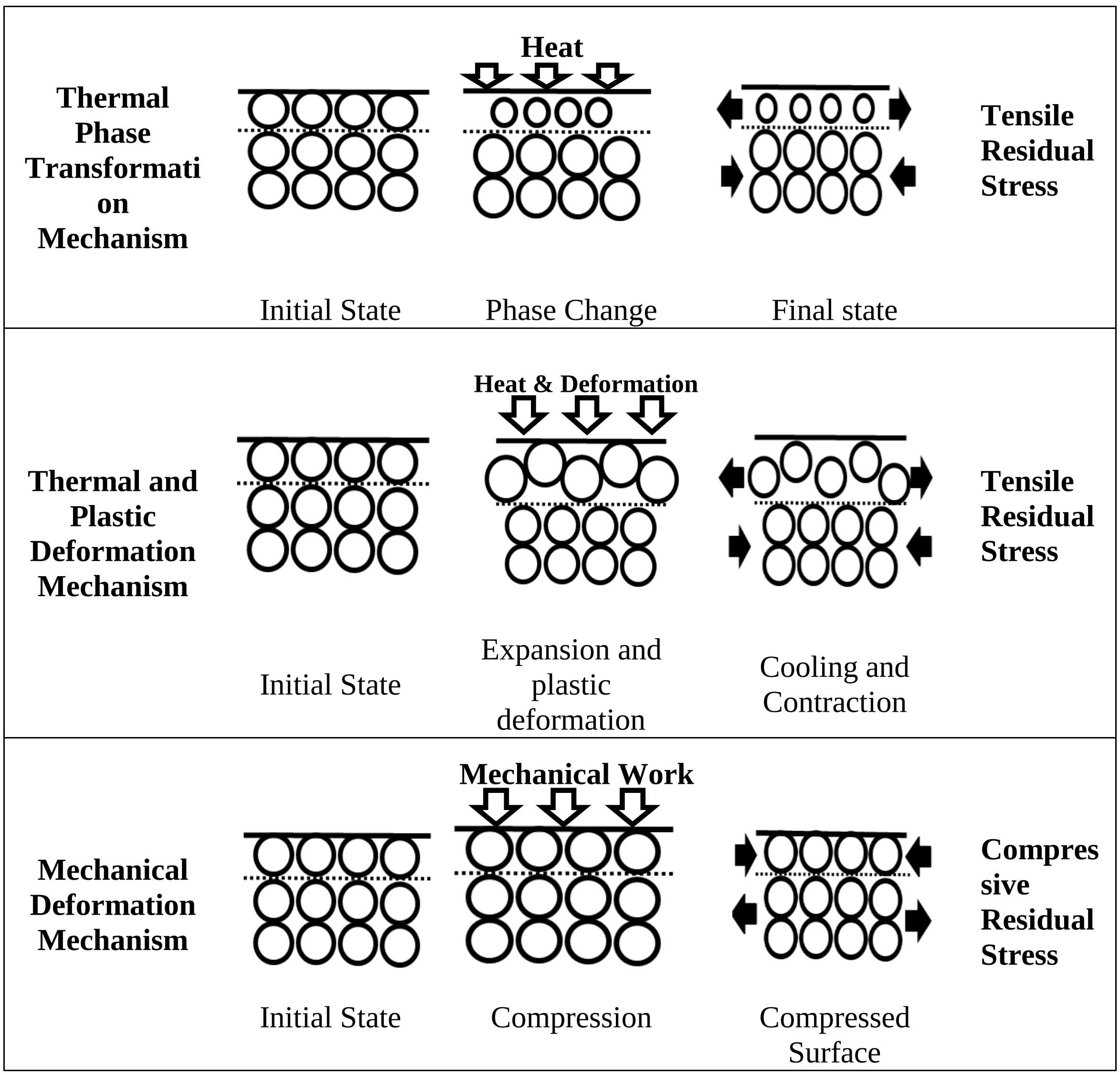

Figure 2-12: Residual stress models (Grzesik, 2008)

Surface integrity study in machining H13 tool steel

When machining, it is important to maximize the material removal rate while at the same time it is essential to monitor the quality of the machined surface by measuring surface roughness, residual stress, and microstructure [Srivastava, Joshi, and Shivpuri, 2004]. In general it is favourable to get surfaces with compressive residual stresses, as parts with high compressive stresses have been shown to have better fatigue life and experience less problems due to crack propagation [A. Vyas, 1999; M.A. Elbestawi, A.K. Srivastavi, 1996; M.C. Shaw, 1993] When machining, the material is stretched, hence the bulk material underneath remains elastic and tries to return to its original state, creating compressive stress. However, with heat generated during machining, tensile stresses are also likely to be found, especially if a large proportion of the heat that is generated during cutting, due to the rubbing of the flank face against the workpiece is directed into the workpiece [Tönshoff, Arendt, and Amor, 2000]. Cutting parameters affect the rate of plastic deformation, hence the mechanical loading experienced by the tool. It is reported that higher compressive stresses can be obtained by aggressive feeds [König, Klinger, and Link, 1990]. It is also found that a higher feed rate and larger negative rake angle produces higher compressive stress [Dahlman, 2004]. [Axinte and Dewes, 2002] reported that cutting speed, feed, tilt angle and depth of cut are some of the parameters which can influence the residual stresses in high speed machining of H13 steel. Zhang et al. [Zhang, Ding, and Li, 2012] studied the residual stress distribution on a machined H13 workpiece when hard milling. It was reported that the distribution of residual stresses were periodic from each pass which took a hook shaped profile with maximum stresses at 3-18 microns depth into the surface. The surface roughness value (Ra) during dry hard milling was reported by [Li, Guo, and Guo, 2013]. It is reported that Ra is reliant on the feed rate and step over, and the condition of the tool had no influence on R_a for flank wear up to 0.2mm. It was found that the residual stresses were compressive with relatively higher stresses in the step over direction than in the feed direction [Li et al., 2013; Zhang et al., 2012].

2.4 Chips

2.4.1 Mechanism of chip formation

In metal cutting there are typically four chip formation mechanisms that can be observed: discontinuous, continuous, and continuous, with built-up edge and serrated edge Figure 2-13. These mechanisms are depended on factors such as tool design, workpiece material property and cutting parameters. [Stephenson and Agapiou, 1997]

Continuous chips don't have a localized shear zone and are instead shearing continuously. They are very commonly found in high speed cutting where the heat enhances the ductility of the chip [Elfizy, 2008]. Continuous chips with built-up edges are found where the material adheres onto the cutting edge. Discontinuous chips are very commonly seen for brittle material. They have also been reported in dry machining on ductile material at low speeds [Armarego and Brown, 1969].

Serrated or saw tooth chips have very localized shear planes and are commonly seen in high speed machining of hardened tool steel. Formations of saw tooth shaped chips are based on the following two theories, “Adiabatic shear theory” and “Crack propagation theory”. Adiabatic shear theory is based on catastrophic thermoplastic instability. High cutting speed causes an increase in thermal softening. This also causes the strain rate to increase, however a lot of localized heat present in the cutting zone causes the rate of thermal softening to exceed the rate of strain hardening, leading to catastrophic shear slip [Davis et al., 1996; Chen et al, 2004]. Crack propagation theory states that the localized shear plane is due to cyclic cracks which propagate though the free surface. The free surface is where the least compressive stresses are found. Micro-cracks are initiated due to the presence of voids, dislocations and other imperfections. These cracks start to propagate towards the tool tip leading to a localized slip plane [Nakayama, et al. 1996; Shaw and Vyas, 1993; Elbestawi et al., 1996].

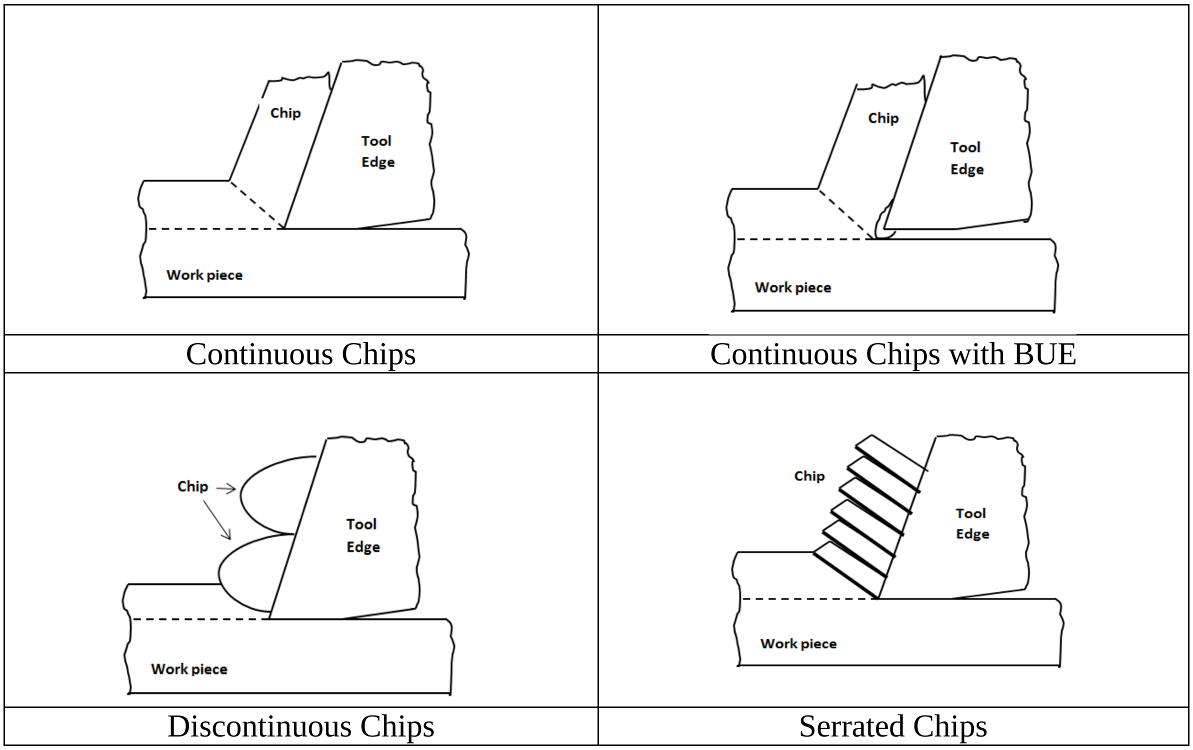

Figure 2-13: Chip Formation Mechanism (Stephenson and Agapiou, 1997)

2.4.2 Chip color estimation

The dynamics of metal cutting make it very difficult to measure temperature using external devices. One of the approaches researchers have taken is by trying to link the color of the chips with cutting temperature. Table 2-8 illustrates a summary and comparison of several author's research on linking chip color to cutting temperature

Table 2-8: Chip Color VS Chip Temperature [Ning et al., 2001; Ning, 2007]

	[Ning et al., 2001]	[Ning, 2007]
Color of chip	Temperature (ºC)	
Light Brown	800-840	-
Brown or Golden brown	820-880	-
Blue + Brown	860-920	-
Light blue	-	-
Blue Purple	920-960	-
Dark Blue	960-1000	-
Dark Blue + Green	>1000	-
Green + Silver		>1100
Green + silver + Radish brown		>1100

Chapter 3 Experimental Work

3.1 Experimental Procedure for Tool life study

3.1.1 Tool and workpiece properties

Cutting tools used in this study were micro-grained tungsten carbide ball nose end mills, from Mitsubishi, with high wear resistance and high toughness.

Table 3-1 illustrates the geometry and property of the carbide cutting tool used in this study. The tool is a 2 fluted ball nose end mill with 10mm diameter. The helix angle along the cylindrical part of the tool is 30º and 0 - 27º at the ball part. The microstructure of C-2SB grade consists of a very fine grain, hence giving the substrate a high micro-hardness property of 1950 – 2000HV. The tip of the ball nose end mill is generally at the very center (on the Z-axis) where the cutting speed is zero. The chemical composition of the cutting tool is illustrated in Table 3-2AISI H13 Hot Work Tool/Die was used as the workpiece material for all cutting tests. The composition is provided in Table 3-3.The H13 block on which the cutting test was sent for hardening at 1060ºC, quenched in air followed by tempering at 500 ºC. The workpiece was through hardened to 54-55HRC.

Table 3-1: Tool Geometry and Properties [Elfizy, 2008; Ning, 2007]

Mitsubishi Carbide tool (C-2SB)	
Radius of ball nose (mm)	5
Shank diameter (mm)	10
Flute length (mm)	10
Overall length	100
Number of flute	2
Helix angle (Straight part)	30º
Helix angle (ball part)	0-27º
Microhardness(HV)	1950-2000

Table 3-2: Chemical composition of Mitsubishi ball nose end mill [Ning, 2007]

Elements	**WC**	**Co**	**TaC**
Weight%	89.5	10	0.5

Table 3-3: Chemical composition of H13 tool steel [http://www.matweb.com]

AISI H13	C	Cr	Mo	Si	Mn	V	Fe
Weight %	0.39	5.2	1.4	1.0	0.4	0.9	Rest

3.1.2 Experimental setup for cutting, Cutting parameters and Coatings

Figure 3-1 illustrates the experimental setup. The cutting experiments were performed on the 3 axis vertical milling machine, Matsuura FX-5. The FX-5 has a maximum spindle speed of 27,000RPM, spindle power of 20kW, rapid feed rate of 25m/min with high precision and rigidity. The workpiece was mounted on a Kistler dynamometer 9255B to measure the cutting force signals. A Kistler 5010 charge amplifier was used to amplify the signals during cutting. A National Instruments data acquisition card was used to convert the signals from analog to digital, which was then digitally stored using a custom Labview program. The Labview software was also used to extract the cutting force information from the signals.

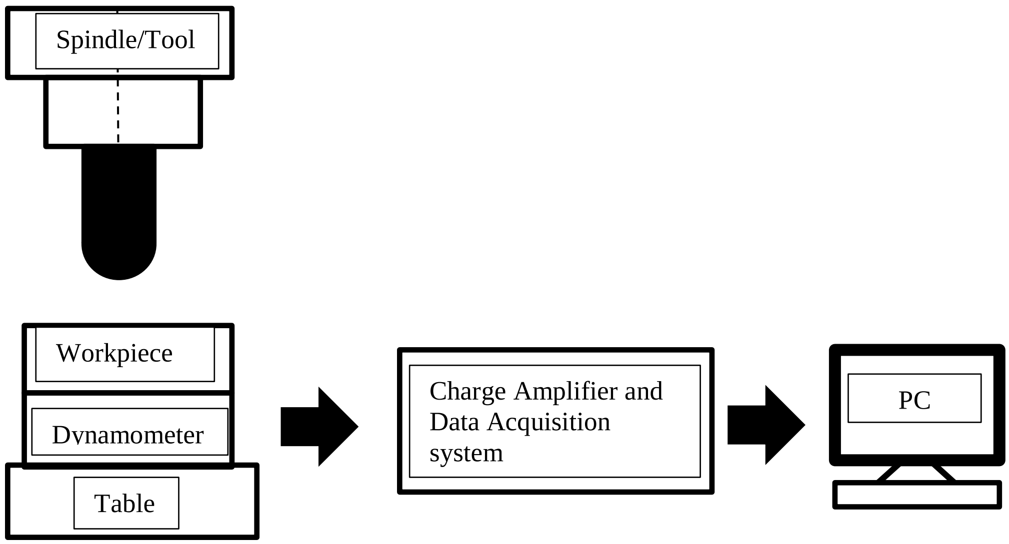

Figure 3-1: Experimental Setup for Cutting Tests

Table 3-4: Cutting Condition

Cutting condition	Dry cutting with Air blasted at 100Psi
Type of milling	Down milling
Tool holder type, Collet	BT plus, NBC20
Force in X direction	Feed force
Force in Y direction	Cutting force
Force in Z direction	Thrust force

The tool was step up on a BT plus tool holder and NBC20 collet. Tool run out and overhang length were measured and recorded with each test since machining was performed at high spindle speed. The overhang length of the tool was kept to a minimum to ensure that the tool deflection does not affect the result. The run out of the tool was also checked using a highly sensitive dial gauge in order to ensure that the load on both flutes was even. The machining was done in a “down milling” manner with the tool path illustrated in Figure 3-2. A straight cutting path was used with no tilt angle.

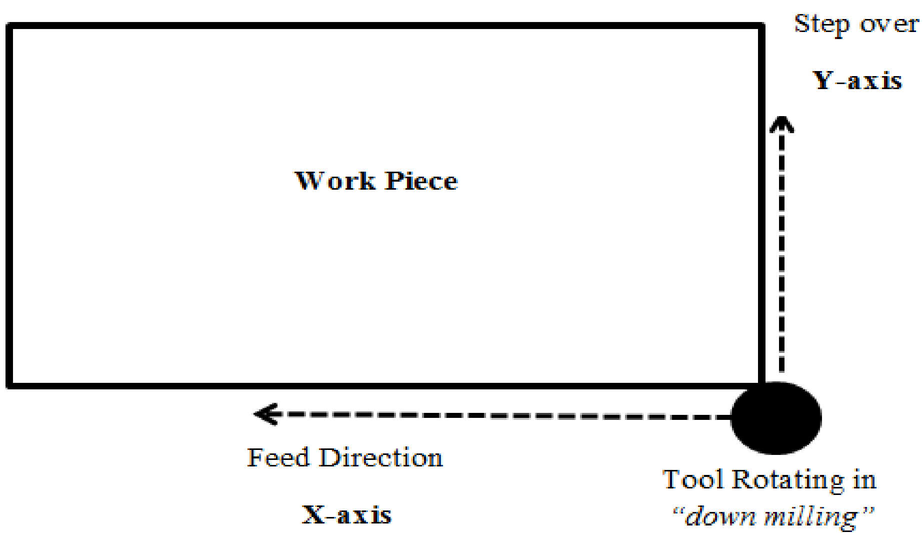

Figure 3-2: Tool Path

The cutting parameters given in the Mitsubishi manual for finish hard milling of H13 with an AlTiN coated tool of 10mm diameter were: 0.3mm axial depth of cut, 0.5mm radial depth of cut and feed per tooth of ≤ 0.125 mm/tooth [http://www.mitsubishicarbide.com]. The final parameters used were chosen for the following two reasons. Firstly it was necessary to study the chips to better understand the cutting process. The chips generated with 0.3mm of axial depth of cut were very small and difficult to analyze. Secondly, the recommended parameters would increase the duration of the experiment beyond what was practically reasonable in terms of time and material consumed. For these reasons the feed rate, radial and axial depth of cut were altered as suggested in the literature, to study the cutting performance while maintaining high material removal rates (Ning, 2007; Elfizy, 2008). The final cutting parameters used for studying the performance of the different coatings are illustrated in Table 3-5.Table

3-6 and Figure 3-3 illustrate the cutting parameters and provide a schematic of the accelerated tool life tests performed on the TiAlCrSiYN/TiAlCrN coated tools.

All tools were PVD coated with different compositions prepared by Kobelco a division of Kobe Steel Ltd. The tools were heated to around 500 °C and were cleaned with Argon etching for 7.5min. Ar-N_2 gas was fed into the chamber at a pressure of 2.7 Pa. Different coating targets were supplied by material vendors and were manufactured by powder metallurgical processes. The coating was then deposited using a plasma arc source for 20 minutes. Deposition was done with a Bias voltage of 100V and the sample was rotated at 5 rpm resulting in a 2 micron thick coating.

During tool life testing, the cutting tools were periodically examined under an optical toolmaker microscope (Mitutoyo TM) to measure and track the flank wear, rake wear and chipping. Based on ISO 8688-1 criteria, end of tool life was determined when the tool flank wear reached 0.3mm.

Table 3-5: Cutting parameter for tool life testing of coating

Test	Coating	Cutting Speed (m/min)	Feed per tooth (mm)	Axial depth of cut (mm)	Radial depth of cut (mm)
1	TiN	500	0.06	5	0.6
2	TiAlN	500	0.06	5	0.6
3	TiAlCrSiYN	500	0.06	5	0.6
4	TiAlCrSiYN/ TiAlCrN	500	0.06	5	0.6

Table 3-6: Cutting parameter for the accelerated test with TiAlCrSiYN/TiAlCrN

Test	ID	Cutting Speed (m/min)	Feed per tooth (mm)	Axial depth of cut (mm)	Radial depth of cut (mm)
1	600 (Benchmark)	600	0.06	5	0.6
2	600_700x1	600/700	0.06	5	0.6
3	600_700x2	600/700	0.06	5	0.6
4	600_700x3	600/700	0.06	5	0.6
5	700	700	0.06	5	0.6

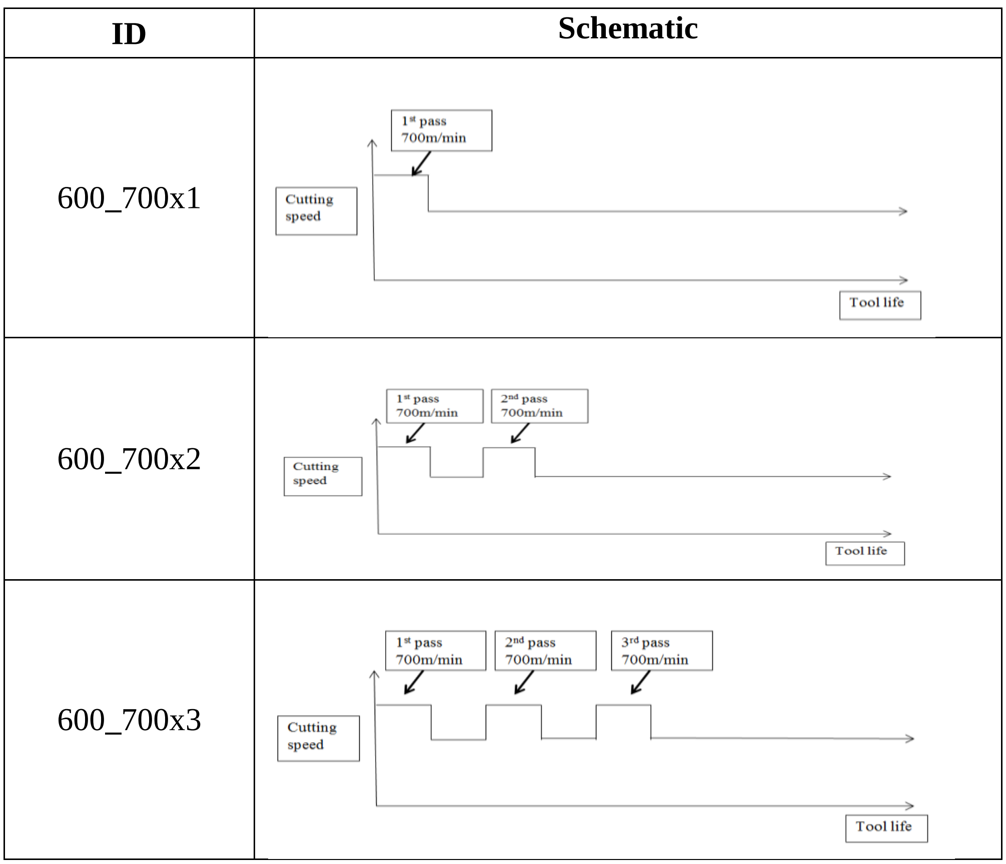

Figure 3-3: Schematic of the accelerated tool life test conditions

3.2 Experimental procedure for Surface Integrity

3.2.1 Preparation and Characterization of TiAlCrSiYN/TiAlCrN and TiAlCrN Coated Tools

The coatings outlined in Table 3-5 were compared to the tribological behaviour of the top commercially available coating (TiAlCrN). In all cases the coated tools were run for a 100m machining length mark. The following machining procedure and parameters were used: speed of 500m/min, axial depth of cut = 5mm, radial depth of cut = 0.6mm, and feed per tooth = 0.06mm. A JEOL 6610V scanning electron microscope (SEM) was used to provide images at different stages of tool life (0m, after 2m, 15m, 30m and 100m) to track the wear. Prior to capturing these images, the tools were cleaned in a sonicator with acetone solution. The inspection site was then blasted with clean pulsating air to blow away any debris. Finally the sample was mounted on a specially designed tool holder fixture to ensure that the tool is held in the ideal orientation inside the SEM chamber for inspecting the cutting edge.

X-ray Photoelectron Spectroscopy

The tool was cut using an electro discharge machine (EDM) so it could be analyzed using X-ray Photoelectron Spectroscopy (XPS), Figure 3-4**.** XPS experiments were performed on a Physical Electronics (PHI) Quantera II spectrometer. The machine uses an Aluminum anode source for X-ray generation and a quartz crystal monochromator for focusing the X-rays. The system's base pressure was less than 1.0 x 10^{-9} Torr and operating pressure less than 2.0 x 10^{-8} Torr. General and high resolution spectras were obtained with pass energy of 280eV and 55eV. All spectra were obtained at a 45º take off angle and used a dual beam charge compensation system for neutralization. The system was calibrated on a clean Silver (Ag) sample where the Ag 3D peak had a binding energy of 368.3 ± 0.1 eV and full width half maximum (FWHM) was at least 0.52 eV. A PHI MultiPak Version 9.4.0.7 software package was used for data manipulation.

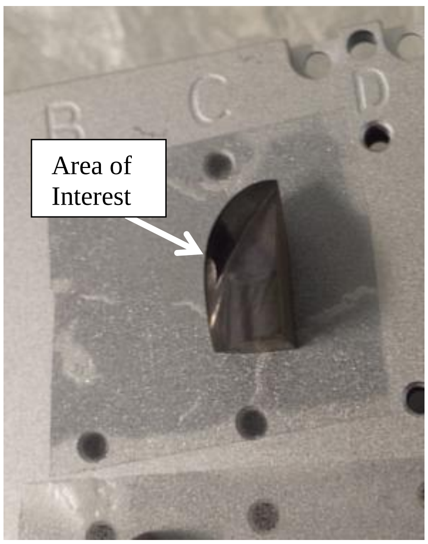

Figure 3-4: XPS sample for analysis

3.2.2 Preparation and Analysis of 3D blocks

Small sample blocks were prepared to study the impact of tool orientation on surface integrity. The 2 coated tools (TiAlCrSiYN/TiAlCrN and TiAlCrN) which were earlier worn to 100m linear length of machining were used to study the 3D block surface integrity.

The 3D blocks were prepared from the same H13 material. The shape of the block was first rough cut out using a water jet machine with a feed rate of 100mm/min. The machining setup for the 3D block was similar to the one used in the previous experiments. The 3D block was then machined several times using a new tool for preparing the surface (total of 1.5mm depth of material was removed from each orientation) to ensure the elimination of any mechanical damage induced by water jet cutting as well as to remove any embedded garnet particles that may be imbedded in the surface during waterjet machining. After this preparation the final test tooling was used as shown in Figure 3-5. The 3D blocks were then machined, using the experimental tools (the 2 coated tools at 100m), several passes were made till a total of 1.5mm depth of material was removed from each orientation. Cutting forces were collected 7 times for each orientation and averaged. Details on the machining of a 3D block and its cutting force orientations are provided in Table 3-7.

Table 3-7: Machining details for the small sample 3D block

Coatings used for Machining 3D block	1. TiAlCrSiYN/TiAlCrN 2. TiAlCrN
Cutting Speed[m/min]	500
Feed per tooth[mm]	0.06
Radial Depth of Cut[mm]	0.6
Axial Depth of Cut[mm]	0.5
Angles studied	0 degree, 15degree, 45 degree and 85 degree
Force in X direction	Feed force
Force in Y direction	Cutting force
Force in Z direction	Thrust force
Dimension of 3D block [Height, Width, length]	25mm, 26.7mm, 30mm

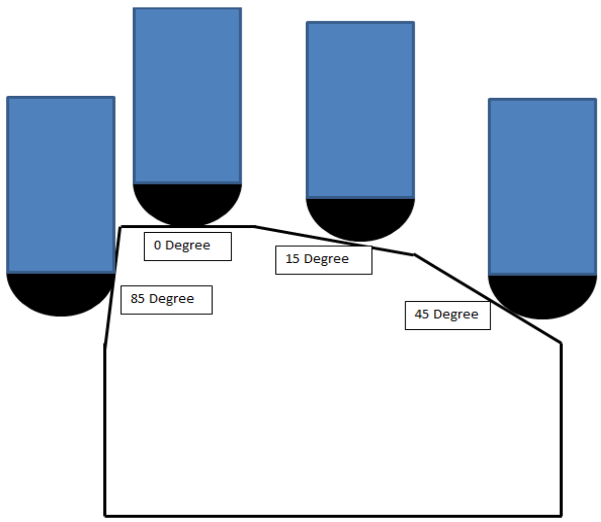

Figure 3-5: Machining at different tool orientation angles.

Once the 3D block had been machined, surface roughness was measured using a Zygo New View 5000 optical profiling system, which uses white light interferometry. Surface roughness was measured in the pick direction (step over direction). Images of surface topography were also taken using a Nikon Stereoscope microscope at different magnifications. XRD was performed to measure surface residual stresses. Figure 3-6 illustrates the points of analysis for surface residual stress. The 3D blocks were then cut using wire EDM and cold mounted, exposing the cross section of the machined surface. The samples were ground, polished, and etched using 2% nital solution. SEM images were taken to study the microstructure of the machined surface.

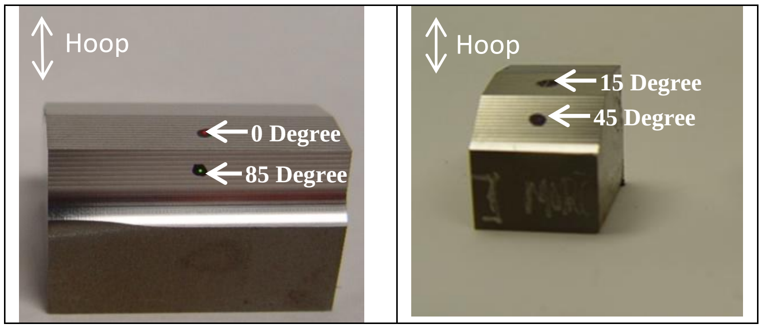

Figure 3-6: Points of analysis for surface residual stress.

3.3 Chips

In order to compare the effect of tool workpiece tribology on the cutting process, chips from the cutting with the TiAlCrN and TiAlCrSiYN/TiAlCrN coated tools were collected at different stages (2m, 15m, 30m and 100m) while the tool was being worn in preparation for machining the 3D blocks. To study the under-surface, chips were analyzed under a SEM. Chips were mounted on stubs using carbon tape, and sputter coated with gold (36nm). Cross sections of these chips were prepared by cold mounting under high vacuum in epoxy resin. The samples were then ground using SiC paper, followed by polishing and finally etched using 2% nital solution to study the chip formation mechanism and micro-hardness. The colors of the chips were also investigated to give an approximate cutting temperature. A Canon T3i DSLR camera was used to observe and capture the color images.

Chapter 4 Results and Discussion

4.1 Impact of Tribosystem on Tool Life and Tool Wear

Cutting H13 at high speed under the given test parameters requires excellent protection performance from the coating. Figure 4-1 illustrates the tool life of the ball nose end mill with different coatings at 500m/min. It is seen that the TiN coated tool only machines 27m of linear workpiece length. The addition of Aluminum (Al), Chromium (Cr) and Silicon (Si) alloying elements in the TiAlCrSiN coating significantly increased the tool life from 27m to 213m for the TiAlCrSiN coating. The inclusion of the additional alloying element Yttrium (Y) further enhanced life to 224m for the TiAlCrSiYN coating. The largest improvement in tool life was seen by structuring the coating in a multilayered manner, with alternating layers of TiAlCrSiYN and TiAlCrN coatings resulted in a drastic increase in tool life to 411m of linear machining length.

The structure of the underlying TiN coating is characterized as a binary multi-component coating. The addition of Al as an alloying element greatly improved the hot hardness and promoted the formation of Aluminum Oxide (Al_2O_3) on the surface of the tool. Al_2O_3 is characterized as an ionic compound with high hardness, low thermal conductivity and high thermal stability. The addition of Al is also believed to delay the temperature where the onset of rapid oxidation takes place from 600ºC for TiN to 950ºC for TiAlN [Zhou, et al., 1999]. The addition of alloying elements such as Cr and Y helps in further enhancing the coating properties by improving oxidation and corrosion resistance [Smith et al., 1997]. The inclusion of Cr allows for the formation of Cr-oxides on the surface of the tool, which can act as a solid lubricant [Fox-Rabinovich et al., 2005], whereas the presence of Y delays the temperature at which rapid oxidation initiates [PalDey and Deevi, 2003]. The addition of Si allows for the further increase in oxidation resistance and an increase of hardness. Structuring these layers in a multi-layered format as in the case of the TiAlCrSiYN/TiAlCrN coating was found to further enhance tool life. The multi-layered coating is known to have the advantage of reducing grain growth thus resulting in higher hardness. Multilayer coatings are also more resistant to crack propagation by deflecting the cracks laterally along the interface rather than deeper into the coating which would promote delamination [PalDey and Devvi, 2003]. Generally an increase in cutting speed leads to a lower tool life however in one study it was shown that increasing the cutting speed actually led to an increase in tool life [Fox-Rabinovich et al., 2015]. One of the primary factors that a change in cutting speed alters is the contact temperature in the cutting zone and the formation of oxides is highly sensitive to temperature. Typically there are two temperatures associated with oxidation. Firstly, the temperature at which oxidation initiates, and secondly, the oxidation onset temperature where the rate of oxidation rapidly increases and leads to coating failure. Ideally, for a given adaptive coating the cutting parameters should be chosen between these two temperature limits [Ning, 2007]. In addition to establishing the importance of the oxidation rate, it is also important to identify the types of oxides which are forming and understand the critical role they play in determining tool life.

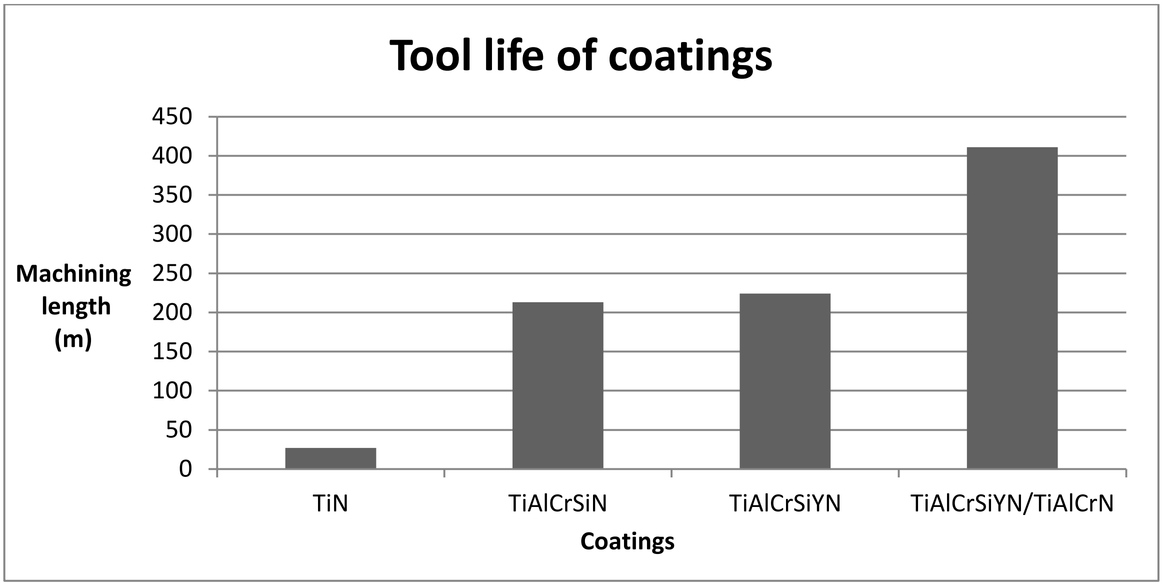

Figure 4-1: Tool life of different coatings at 500m/min [TiAlCrSiYN/TiAlCrN based on, Fox-Rabinovich, 2015]

To understand the mechanism of adaptability and the formation of tribofilms, TiAlCrN and TiAlCrSiYN/TiAlCrN coatings were compared. Both of these coatings were worn to 100m of machining length at 500m/min of cutting speed. The wear patterns for both the tools were tracked and observed using the SEM mentioned earlier. X-ray Photoelectron Spectroscopy (XPS) was also performed on the rake face of the tool to study the formation of tribofilms which play a crucial role in determining tool life. Figure 4-2 compares the flank wear for TiAlCrSiYN/TiAlCrN and TiAlCrN coated tools after 100m of machining. It is seen that after machining the TiAlCrSiYN/TiAlCrN tool has only worn to 52μm whereas the TiAlCrN coated tool has worn to 412 μm. Figure 4-3 and

Figure 4-4 provide SEM images at 100m. It can be observed that prior to machining the TiAlCrSiYN/TiAlCrN coated tool (machining length 0m) has a sharp cutting edge. After 2m, the cutting edge is still intact with a thin layer of material sticking along the edge. There is almost no visible change seen from 2m to 30m which clearly illustrates the effective protection provided by the TiAlCrSiYN/TiAlCrN coating. At the 100m mark, the tool is still relatively unworn with only the very initial signs of wear appearing on the cutting edge.

For the TiAlCrN coating, the tool starts with a sharp cutting edge. However, after only 15m there is relatively more sticking observed, and after 30m, signs of chipping on the tool are visible. As the tool is used to machine 100m length of cut, the tool breaks down rapidly. At the 100m mark the cutting edge has chipped significantly with heavy sticking of the workpiece material observed on the cutting edge. When comparing the condition of the flank face after 100m for both coatings in Figure 4-4, it is seen that the TiAlCrSiYN/TiAlCrN coated tool has managed to withstand the cutting conditions better compared to the TiAlCrN coating.

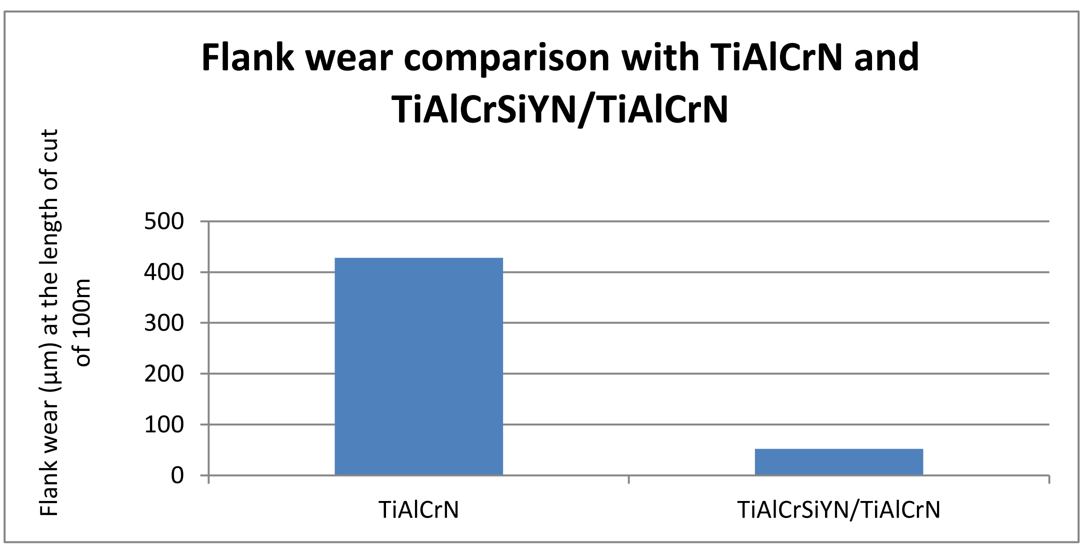

Figure 4-2: Flank wear of TiAlCrSiYN and TiAlCrN coating after 100meter at 500m/min of cutting speed

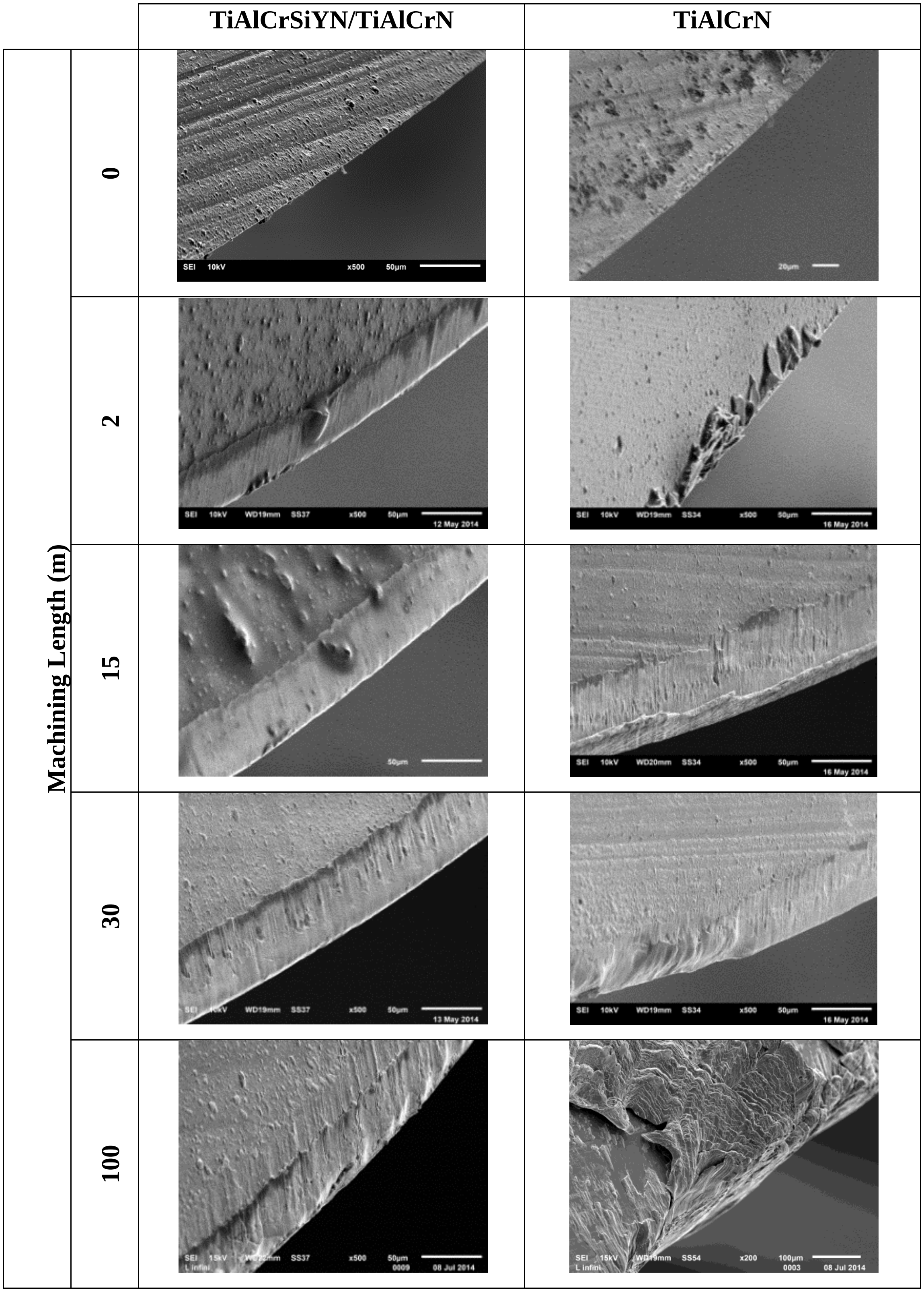

Figure 4-3: SEM images of rake face

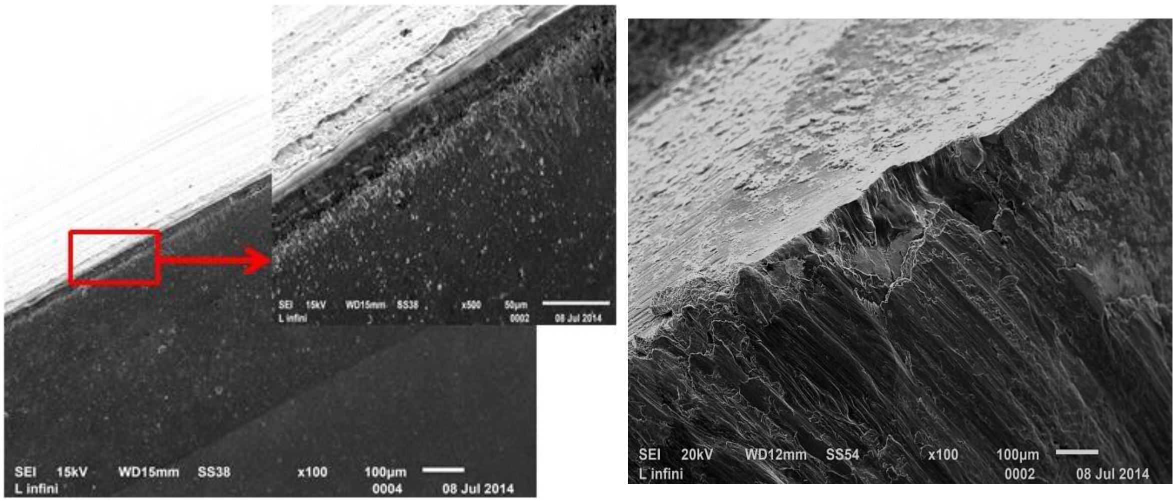

(a) TiAlCrSiYN/TiAlCrN (b) TiAlCrN

Figure 4-4: SEM Image of Flank face at 100m of machining length (a) TiAlCrSiYN/TiAlCrN 100X & 500X (b) TiAlCrN 100X

To understand the mechanism of adaptability and the formation of tribofilms, XPS analysis was performed on both tools worn to 100 meters of machining length. Table 4-1 illustrates the relative ratio calculated using general XPS spectra and high resolution spectra between the different oxides for both coatings. It can be observed that for TiAlCrSiYN/TiAlCrN for every amount of Ti-oxide observed on the surface there is 17.627 times more Al based oxides forming and 12.004 times more Cr based oxides being formed. However for the poorer performing TiAlCrN coating, for every Ti based oxide there is 4.59 times Al based oxides and roughly the same ratio of Cr based oxides. Thus, in the case of TiAlCrSiYN/TiAlCrN coating, the primary protection is provided by the Al and Cr based oxides. Whereas, for the TiAlCrN coating there is significantly less Al and Cr based oxides as compared to Ti based oxides. Based on past experience the Ti based oxides perform well under low cutting temperature, but fail to provide protection at elevated temperature (~1000ºC). The surface was further investigated using high resolution XPS to help understand the structures of each oxides that were generated.

Table 4-1: Relative ratio of oxides after 100m based on XPS

Coating type	**Ti - Oxides**	**Al- Oxides**	**Cr - Oxides**
TiAlCrSiYN/TiAlCrN	1	17.629	12.004
TiAlCrN	1	4.659	1.055

Figure 4-5 and Figure 4-6 show the high resolution spectra from the rake face of TiAlCrSiYN/TiAlCrN and TiAlCrN coated tools after 100m. The TiAlCrSiYN/TiAlCrN coating was investigated based on the intensity of the chart positions based on the locations Ti 2P, Al 2s, Cr 2p, Si 2p and O 1s. Figure 4-5 shows that Titanium can be characterized by a high propensity to oxidize. This leads to the formation of a nonstoichiometric titanium oxide film of 55.2% and TiO_2 (rutile) of 38.5%.Figure 4-5b shows that a major portion of Al has transformed into an Al_2O_3 sapphire like phase. Al has also formed Mullite, which is an Al-Si-O based oxide. Sapphire and Mullite are characterized as refractory compounds. Sapphire is one of the hardest oxides and highly resistant to thermal shock [Scheel and Fukuda, 2003; Lanin, Muravin, popov and Turchin, 2003]. Mullite has similar high temperature properties [Hynes and Doremus, 1991]. Both of these oxides have low thermal conductivity which is especially noticeable at high temperatures compared to a nitride coating [Schulz, 1988; Ditmars, Ishihara, Chang, Bernstein and West, 1982]. They also reduce adhesion between the chip and rake face, hence reducing friction. The formation of Sapphire and mullite is an indication that the cutting process is non-equilibrium and the cutting conditions are harsh. Failure to meet these criteria can lead to the formation of gamma phase Al-oxides which are less protective [Fox-Rabinovich et al., 2012]. Figure 4-5c illustrates the formation of Cr based tribo-oxide films. Cr of different valences have oxidized heavily as observed by summing 88.8 at% and 6.42 at% Cr in nitride. Cr oxides have lubricious properties and can definitely play a critical role in influencing tool wear. Due to the presence of Si in the multilayered coating, Si based oxides were also found as shown in Figure 4-5d. Si-oxides as also known to act as a dry lubricant.

The TiAlCrN coating was investigated using high resolution XPS based on the intensity of the peaks at the position of Ti 2P, Al 2s, Cr 2p and O 1s. Figure 4-6a shows that Titanium has heavily oxidized to form TiO, TiO_2 and Ti_2O_3. Around 19% of the Titanium was seen to result in a nitride form. Figure 4-6b shows that 42.4% of Alumina has oxidized to Al_2O in comparison to 55% Al in the nitride form. Figure 4-6c illustrates that Cr has oxidized to form 77.7% as Cr_xO_y and 17.4% Cr in a nitride form.

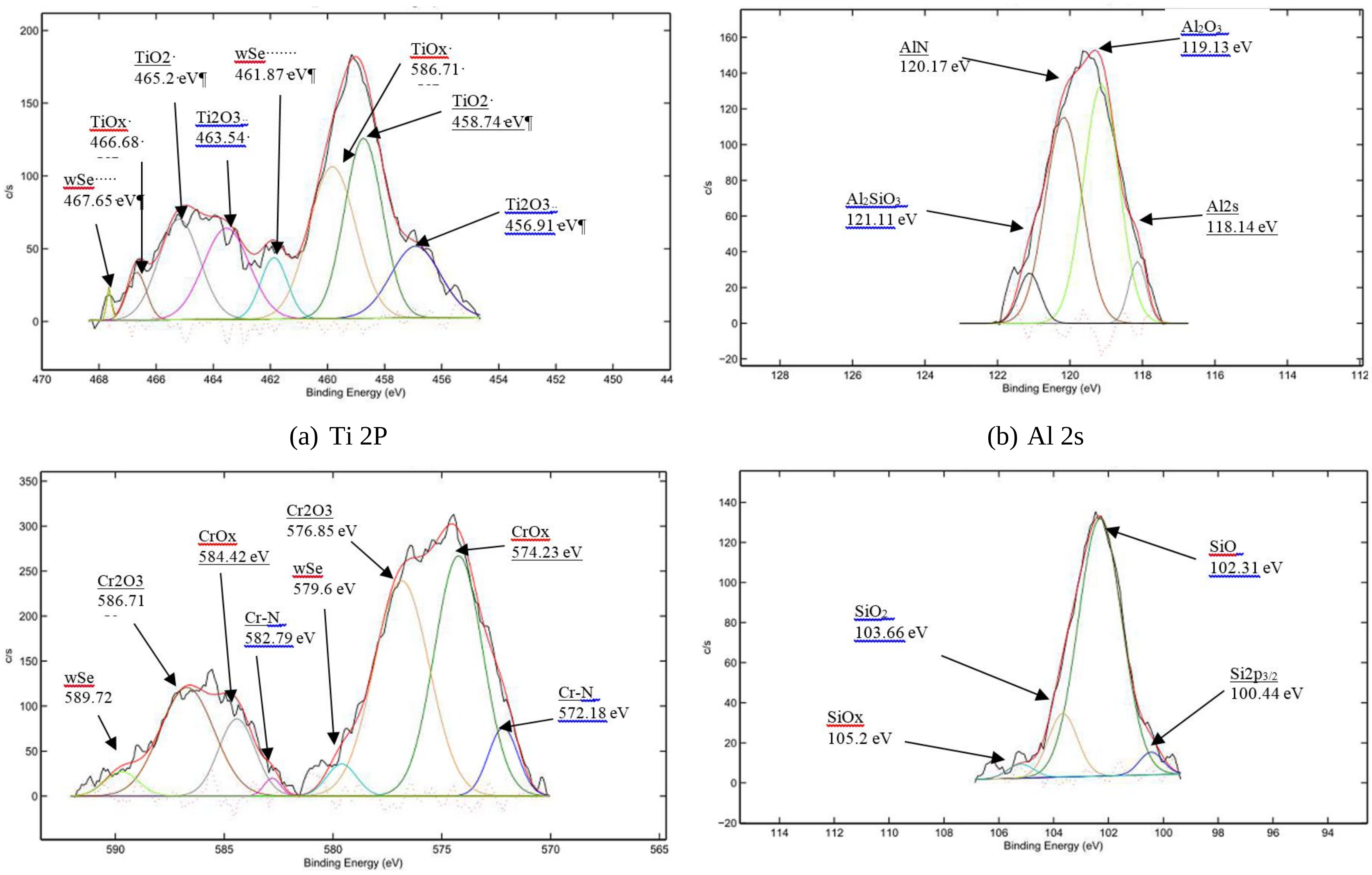

(a) Ti 2P

(b) Al 2s

(c) Cr 2p

(d) Si 2p

Figure 4-5: High Resolution XPS on TiAlCrSiYN/TiAlCrN Coating after 100m

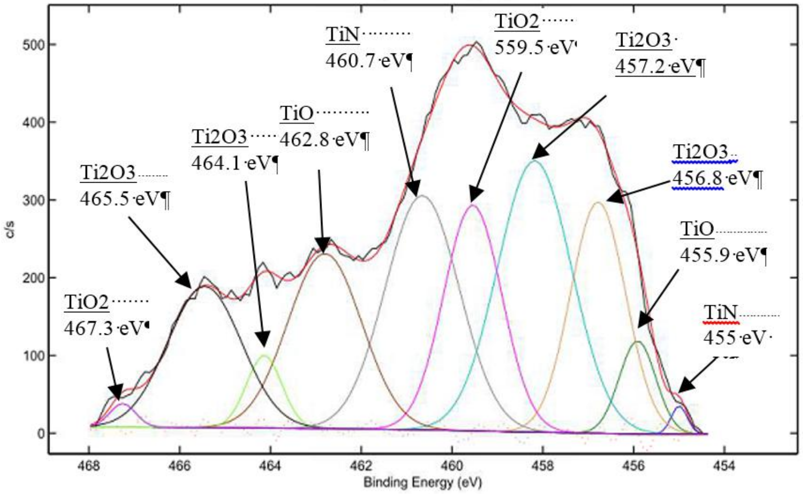

(a) Ti 2P

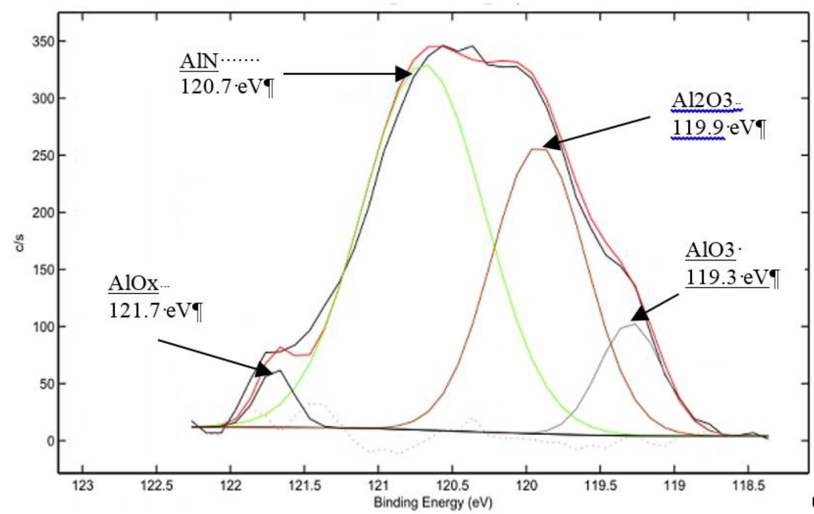

(b) Al 2s

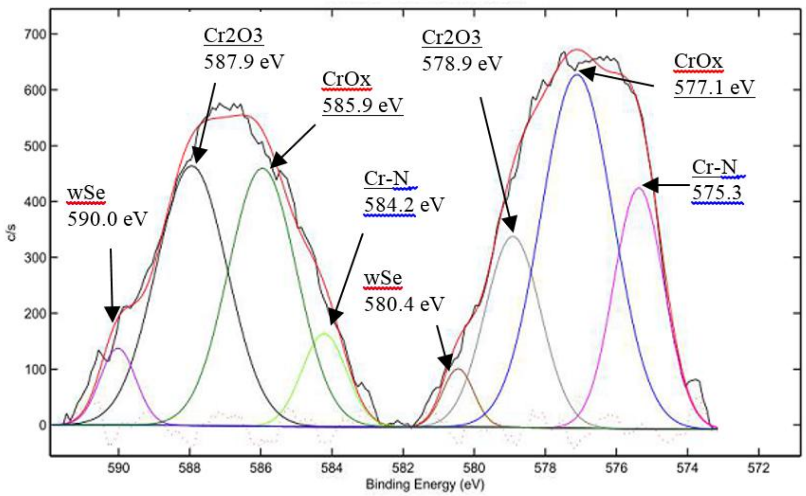

(c) Cr 2p

Figure 4-6: High Resolution XPS on TiAlCrN Coating after 100m

Table 4-2: Microhardness of TiAlCrN and TiAlCrSiYN/TiAlCrN coatings at room and elevated temperature [Beake et al., 2012]

		TiAlCrN	**TiAlCrSiYN/ TiAlCrN**
Grain size (nm)		20-40	20-40
Coating thickness (µm)		2	2
Crystal Structure		FCC nano-crystalline	FCC nano-crystalline
Nano-layer thickness (nm)		-	20-40
MicroHardness (Gpa)	Room Temperature	28.2	30
	450°C	18.5	-
	500°C	-	28
$\mathbf{H^3/E_r^2}$	Room Temperature	0.19	0.27
	450°C	0.06	-
	500°C	-	0.15

The above results demonstrate the importance of carefully selecting the best alloying elements for a coating, such as silicon (Si), chromium (Cr) and yttrium (Y), which have been shown to play a major role in enhancing tool life. The significance of the coating structure is also illustrated where a multilayered coating performs better than a mono layered coating. These coatings are protected by forming oxides, which are constantly being generated and subsequently destroyed during cutting [Fox-Rabinovich and Totten, 2006]. The formation of these oxides is sensitive to the cutting conditions, particularly cutting temperature. Forming of the right type of oxide is crucial as it was seen with the TiAlCrN coatings, where a high ratio of Ti based oxides were formed leading to less protection and thus resulting in more rapid tool wear. TiAlCrSiYN/TiAlCrN coating produces a high amount of Cr and Al based oxides, which provide the tool with excellent protection. [Beake et al., 2012] stated that even though the cutting temperature is approximately 1000°C, The protective tribofilms significantly reduce the heat flux further into the coating and tool substrate material resulting in temperatures just below the thin tribofilm surface layer to be approximately 600°C. The reduction of temperature helps prevent phase decomposition of the coating. [Beake et al., 2012] also reported micro-mechanical properties of TiAlCrN and TiAlCrSiYN/TiAlCrN coatings at room and elevated temperatures, Table 4-2. It is seen that both coatings are hard at room temperature however at elevated temperature TiAlCrSiYN/TiAlCrN was able to retain its hardness whereas TiAlCrN has a severe decline of hot hardness. [Beake et al., 2012] also reported the H^3/E_r^2 ratio, where H is the hardness; E_r is the reduced indentation modulus. Based on nano-impact and nano-scratch experiments researchers found that the TiAlCrSiYN/TiAlCrN deforms in a different manner than TiAlCrN.

TiAlCrSiYN/TiAlCrN has a higher H^3/E_r^2 ratio, indicating lower possibility of crack initiation in the coating. Secondly if a crack does initiate the TiAlCrSiYN/TiAlCrN coating as mentioned previously has the capacity to deflect the cracks laterally along the nano-layer interfaces resulting in less energy for surface damage and also a lowering of the build-up strain leading to sudden failure. In addition to a higher H^3/E_r^2 ratio at elevated temperature, the plasticity of the coating is another important factor to consider in designing a coating for cutting tools. Even though TiAlCrSiYN/TiAlCrN may not have considerably high plasticity, it has been reported that tuning Al% in the coating composition can lead to improvements in tool life [Fox-Rabinovich et al., 2010]. The improved performance of the TiAlCrSiYN/TiAlCrN coating over the TiAlCrN coating is thus attributed to the high hot hardness with its ability to form protective tribofilms, and its beneficial nano-mechanical properties.

4.2 Chip Comparison

To grasp an understanding of the thermal cycle in metal cutting, one of the approaches researchers have taken is to study the chips. This technique has been applied to study chip formation. Predominantly there are three main phenomena in chip formation: strain hardening due to plastic deformation, thermal softening due to heat generation during metal cutting, and quenching when chips are cooled by blowing compressed air in the tool contact zone [Ning, 2007]. By studying the underside surface of the chip, it is possible to study the motion of the chip with respect to the rake face of the cutting tool and chip morphology. The microstructure of the chip's cross-section helps in understanding the chip formation mechanism. Lastly, the inspection of the chip’s color on their underlay surface helps in estimating the amount of heat generated and maximum temperature as well as its effect on the chip micro-hardness along the cross section.

Figure 4-7 and Figure 4-8 show the SEM images of the chip's undersurface, comparing both coatings at their initial stages of tool life and after 100m of cutting. In Figure 4-7, it is observed that at the initial stage the TiAlCrSiYN/TiAlCrN coated tool machines chips with a very smooth undersurface. This is attributed to the fact that the rake face surface of the tool is relatively smooth. After the tool had been worn to 100m, the chips obtained are still very smooth however initial signs of sticking, indicated by the scratch marks on the chips, can be observed as shown in Figure 4-7. Even after 100m of machining with the TiAlCrSiYN/TiAlCrN coated tool, the major mode of chip flow is predominantly sliding.

TiAlCrSIYN/TiAlCrN	
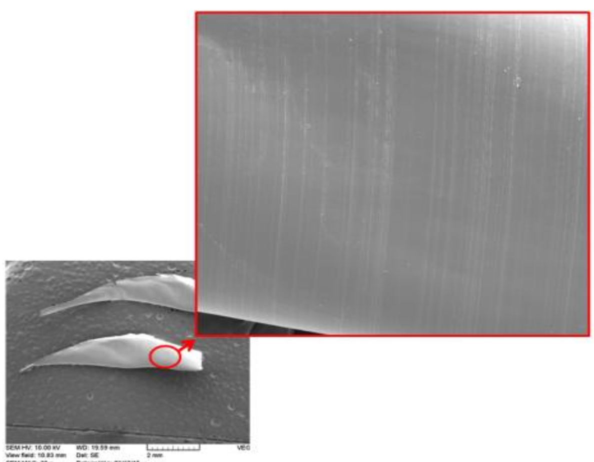	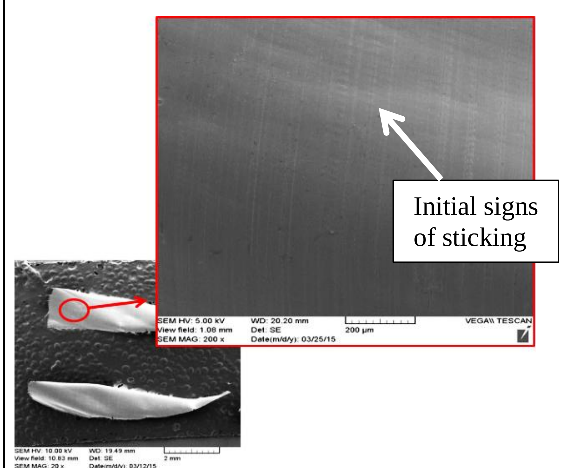
Beginning	**100m**

Figure 4-7: SEM image of chip surfaces with TiAlCrSiYN/TiAlCrN coated tool

Observing chips machined using the TiAlCrN coated tool in Figure 4-8, a smooth surface is seen, however after the tool is worn to the 100m mark, the surface of the chips that are being machined are very wavy. This illustrates that the major mode of chip flow along the rake face is a combination of sticking and sliding. The chips continuously stick on the rake surface and then get released due to a build-up of shear force causing the chips to end up with a wavy surface. After 100m of cutting, it can clearly be seen that the chips have torn and have damaged edges on them. These are attributed to tool wear as the cutting edge breaks down causing the tool to start plowing the material.

TiAlCrN	
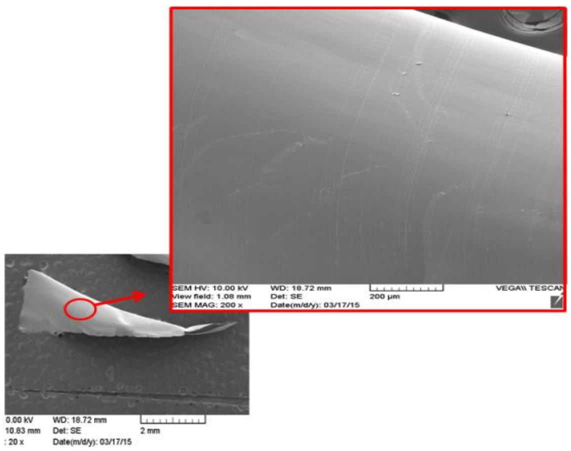	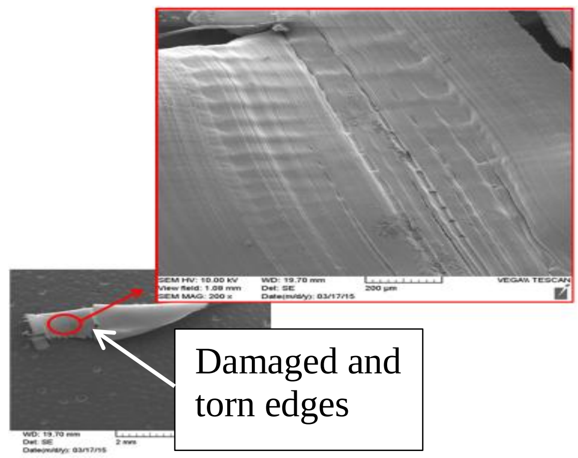
Beginning	**100m**

Figure 4-8 : SEM image of chip surfaces with TiAlCrN coated tool

Next, the cross section of the chip was investigated to understand the chip formation mechanism. Figure 4-9 illustrates the cross section of the chips after 100m for both coatings. It is seen that the chips produced while machining with the TiAlCrSiYN/TiAlCrN coated tool have a saw-tooth shape. The saw-tooth chips are composed of 3 zones as illustrated in the Figure 4-9. These zones being (i) Bulk zone, (ii) Secondary shear deformation zone and (iii) Primary shear zone. The primary shear zones for these chips causing saw tooth shape are localized and well defined. The formation of saw tooth shaped chips is based on two theories. Firstly, "Surface Crack Propagation" theory where the crack initiates at the free surface of the workpiece and grows towards the cutting edge. The crack stops growing at the point where severe deformation of the material exists under high pressure [A. Vyas, 1999; M.A. Elbestawi, A.K. Srivastavi, 1996; M.C. Shaw, 1993]. The second theory is the "adiabatic shearing theory", which states that the main reason for saw tooth chip formation is catastrophic theromoplastic instability [Recht, 1985]. The localized shear plane is expected to get wider and wider as the tool wears. Additionally, the frequency at which the segments are formed is also reported to decrease as the tool wears [Ning, 2007]. This can be clearly seen in the case of the TiAlCrN coated tool in Figure 4-9, where the machined chips are continuous since the cutting tool is worn relatively more. Comparing the secondary shear deformation zone, it can be seen that the width is 2μm and 6μm for the TiAlCrSiYN/TiAlCrN and TiAlCrN coated tools, respectively. As the tools wear, the secondary shear zone gets wider, which indicates an increase in the frictional force resulting in more heat generation [Ning, 2007].

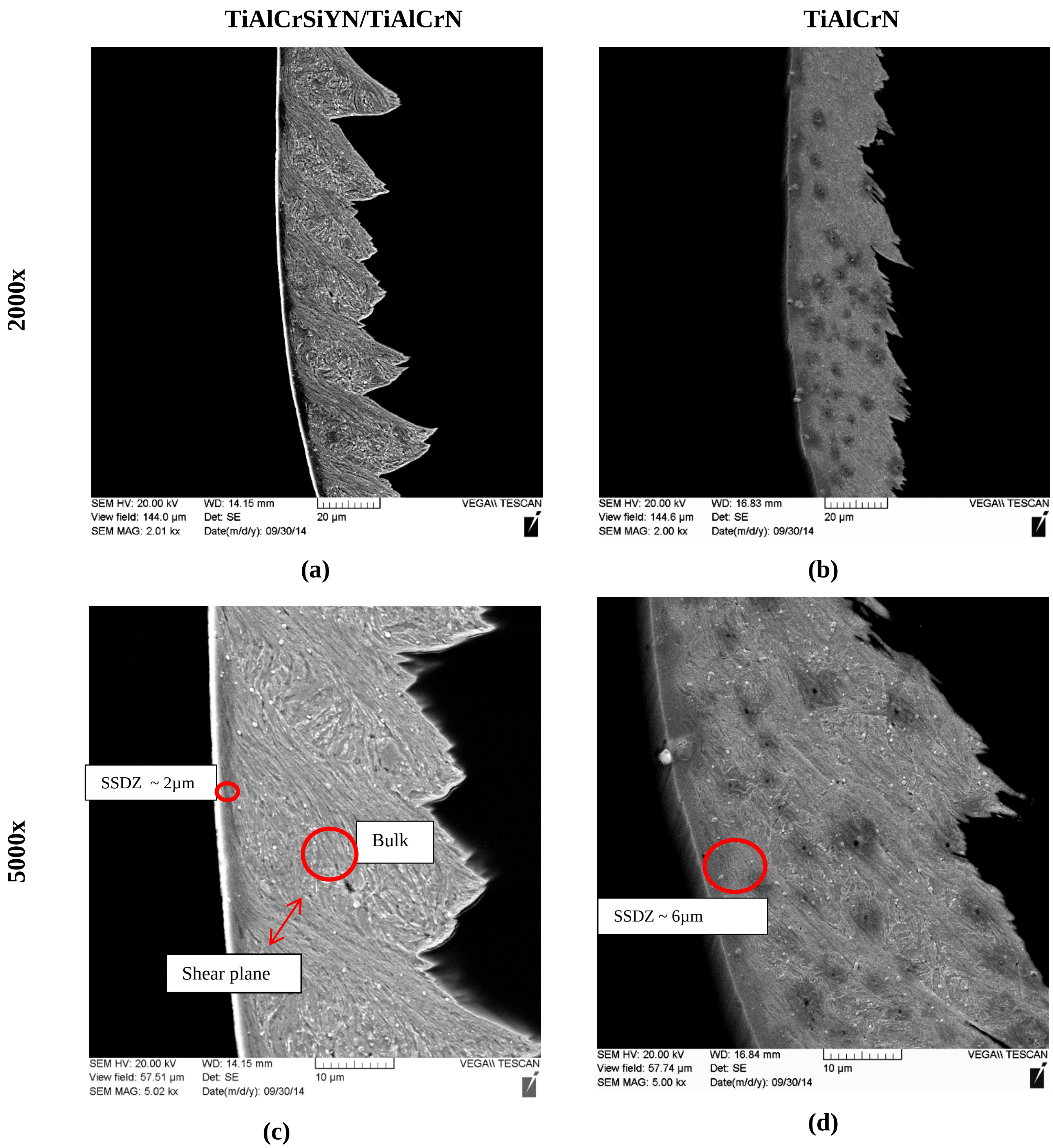

Figure 4-9 : SEM images of chips at 100m of cut, 2000x &5000x.

In milling, the nature of cutting is very dynamic as the tool is constantly engaging and disengaging from the workpiece, making it very difficult to get temperature readings using infrared technology. One of the techniques researchers have adopted is looking at the color of the chip's under-surface to get an estimate of cutting temperature as discussed earlier. Figure 4-10 illustrates the color of the chips at different stages of machined lengths to estimate the machining temperature.

The trend is very similar for both coatings, and as the machined length increases more heat is generated due to the geometry of the worn tool. However, the amount of heat being generated at each stage is dependent on the state of the cutting tool and the coating properties. It can be observed in Figure 4-10 for TiAlCrSiYN/TiAlCrN coating that it starts with "brown purple" chips having an estimated temperature of 860-920ºC. As the tool wears out, the temperature increases with changes in color being observed. After 100m, the chips are heavily oxidized and the interface temperature was estimated as being above 1000ºC. As for the TiAlCrN coating, it too starts off with "brown purple" chips representing an estimated temperature of 860 -920ºC. However, after 100m, the chips from the TiAlCrN coated tool were "silver + blue + purple + brown" having an estimated temperature greater than 1100ºC. Thus the heat being generated is definitely dependent on the degree the tool has worn. In addition, the coating itself plays a major role in determining the level of wear and also on the tribological conditions in the contact zone. Both coatings function by forming oxides on the tool surface. These oxides have lubricious properties as well as thermal barrier properties. The type and amount of oxides are controlled by the coating composition. Definitely, the heat that is being generated does alter the chip's property and it is something important to consider when assessing the performance of a tool.

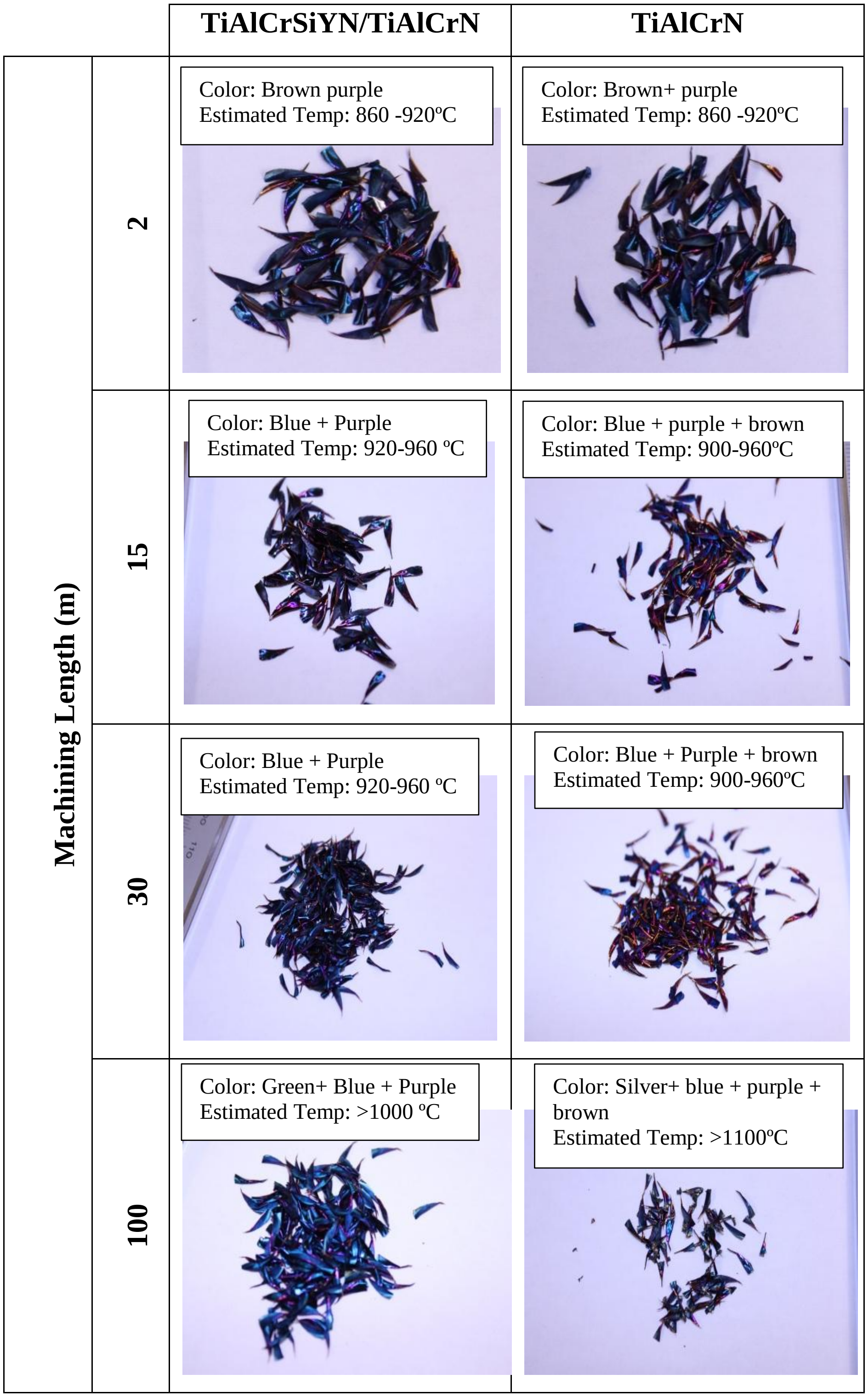

Figure 4-10: Chip color and estimated temperature

Figure 4-11 illustrates a comparison of micro-hardness on the chip cross section for both coatings. It can be seen for both cases that the material is softer near the secondary shear deformation zone (SSDZ) as compared to the bulk of the chip. This is because the SSDZ of the chip is exposed to heat from the rake face and chip interaction thus causing thermal softening. The Vicker's hardness of the chips for the TiAlCrSiYN/TiAlCrN coating at two locations is 494HV (49.2 HRC) and 658HV (56.9HRC). For the TiAlCrN coating, the hardness at similar locations is 668HV (57.7 HRC) and 724HV (59.5HRC). The difference in hardness is due to the fact that the chips for the TiAlCrSiYN/TiAlCrN coated tool undergo strain hardening due to plastic deformation. In addition, the presence of thermal protective tribofilms causes thermal softening as heat is directed to the chips. For the TiAlCrN coated tool, a temperature in excess of 1100ºC is reached, which is higher than the austenization temperature, [Robert et al., 1998] causing the chips to be hard and brittle after it experiences rapid quenching due to the forced air cooling.

<table>
<tr><th>TiAlCrSiYN/TiAlCrN</th><th>TiAlCrN</th></tr>
<tr><td>
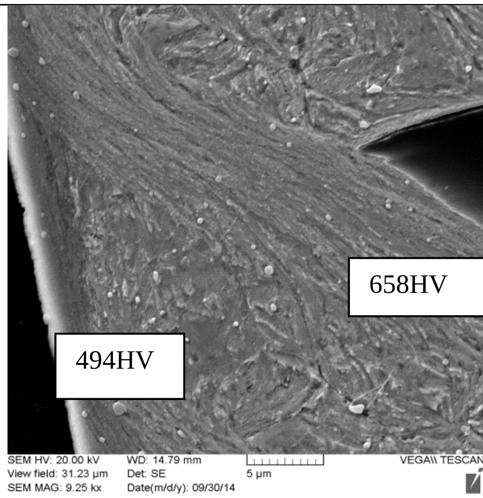

</td><td>
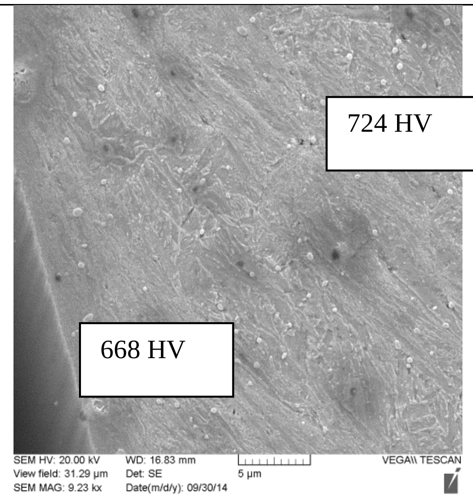

</td></tr>
</table>

Figure 4-11 Chip Micro-Hardness (a) TiAlCrSiYN/TiAlCrN (b) TiAlCrN

4.3 Surface Integrity

Surface integrity of the machined surface was studied using both coatings (100m worn tools) at different tool orientations. With the help of CAD software, the cutting speed for a given orientation was inspected. Figure 4-12 shows the minimum cutting speed ($V_{min,}$), maximum cutting speed (V_{max}) and cutting speed range (ΔV) for the given cutting parameter. Cutting speed is a function of tool diameter and RPM, *Cutting speed= Pi × Tool Diameter × RPM.* Since the RPM is constant in our case, cutting speed is a function of only the tool diameter. Naturally, one can expect the cutting speed to be slower when closer to the axis of rotation (z-axis) and faster when further away from the z-axis. Figure 4-12 shows that the cutting speed is zero at 0 degrees and at its maximum for the tool angle of 85 degrees. Also, it is observed that the difference between the maximum and minimum cutting speed (ΔV) is 5.8m/min when the tool is at 85 degrees, the smallest range studied. As Machining is done closer to the tip of the tool for the 0 and 15 degree tool angle case the cutting speed range (ΔV) increases, being as high as 217 and 226m/min respectively along the tool-workpiece contact line. In Sections 4.3.1 - 4.3.3 the impact on surface topography, microstructure and surface residual stresses of engagement angle of the tool at different orientations was studied.

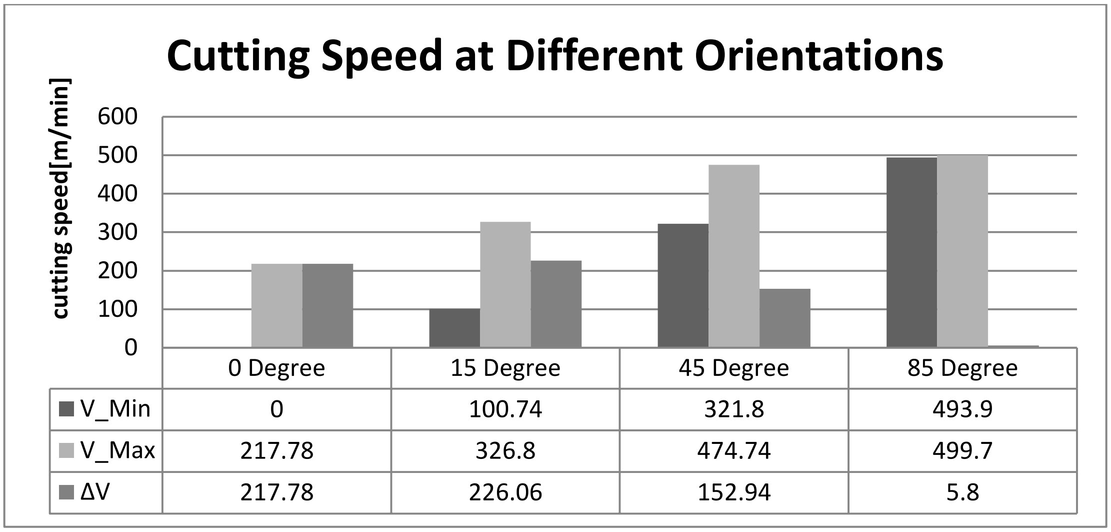

Figure 4-12: Effective cutting speed at different orientation for 0.5 mm DOC and 0.588 mm radial DOC

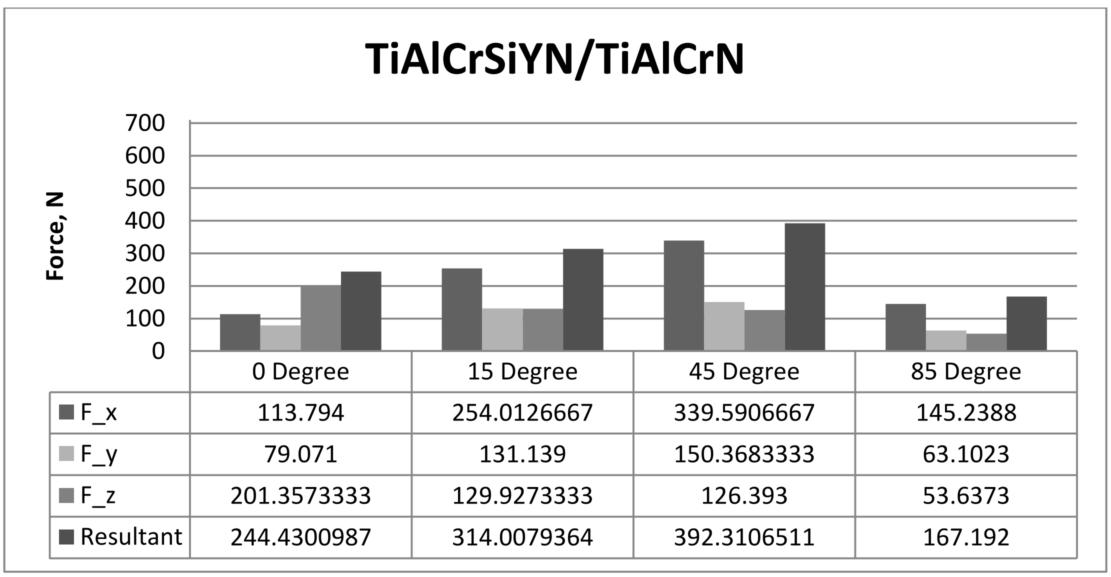

Figure 4-13: Force analysis with TiAlCrSiYN/TiAlCrN coating at different orientation after 100m.

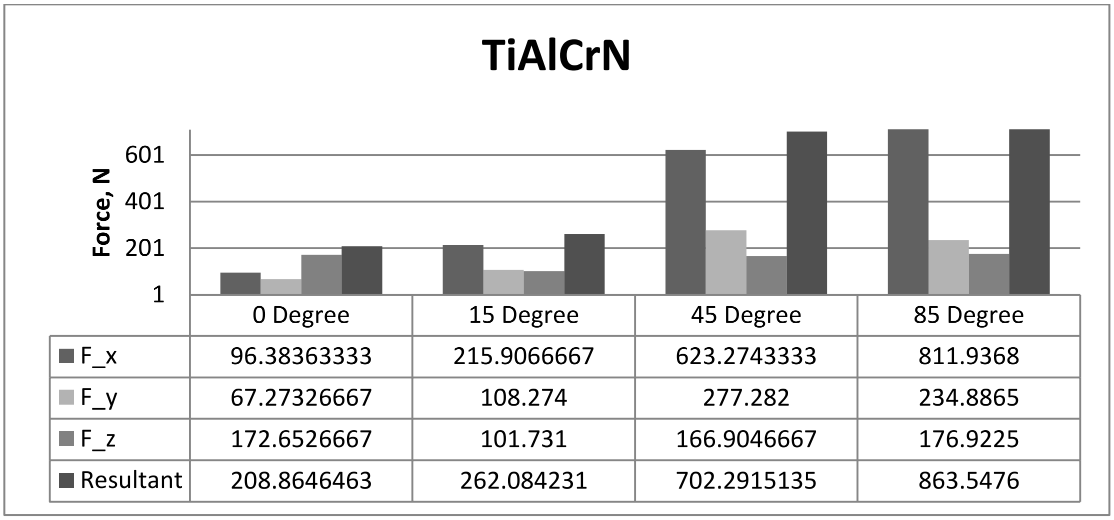

	0 Degree	15 Degree	45 Degree	85 Degree
F_x	96.38363333	215.9066667	623.2743333	811.9368
F_y	67.27326667	108.274	277.282	234.8865
F_z	172.6526667	101.731	166.9046667	176.9225
Resultant	208.8646463	262.084231	702.2915135	863.5476

Figure 4-14: Force analysis with TiAlCrSiYN/TiAlCrN coating at different orientation after 100m.

4.3.1 Surface Roughness and topography

Studying surface roughness and surface topography gives a physical meaning to the quality of the machined surface. Figure 4-15 and Figure 4-16 show Zygo images (white light interferometer) and 3D microscope images at different orientations for both coatings. It is seen in Figure 4-15, for the TiAlCrSiYN/TiAlCrN coated tool at 0 degrees, the R_a of the machined surface is 6.06µm. At 15 degrees, R_a=2.11 µm, 45 degree R_a=2.23 µm and at 85 degrees, R_a=2.52 µm. The sudden decrease in surface roughness from 0 degrees to 15 degrees is due to the change in the material removal mechanism from plowing at the zero cutting speed point to cutting along the edge of the tool. It can also be observed in the Surface topography image in Figure 4-15, the smearing and ploughing effect of machining with the tool tip. Since at 15 degrees the cutting speed is a lot higher, the machined surface is a lot cleaner, hence lower surface roughness. At 15 degrees, the speed band (ΔV) is high, hence one can observe the resulting change in surface topography.

Figure 4-16 illustrates the surface roughness and surface topography of the machined surface using the TiAlCrN coating. Once again, it is seen that at 0 degrees the tool tip is plowing the material hence having similar roughness of R_a=6.03µm. A similar shift in material removal mechanism from ploughing to cutting is observed when shifting from 0 degrees to 15 degrees. At 45 degrees, R_a=2.22 µm with the small amount of material being left on the surface attributed to tool chipping. At 85 degrees the surface roughness is worse with R_a=12.65 µm. The TiAlCrN coated tool chipped heavily at the outer most radius where the cutting speed and chip load were maximum. Since the width of the chipped edge is greater than the step over size at 85 degrees, it caused the tool to machine straight steps rather than scallops at 85 degrees.

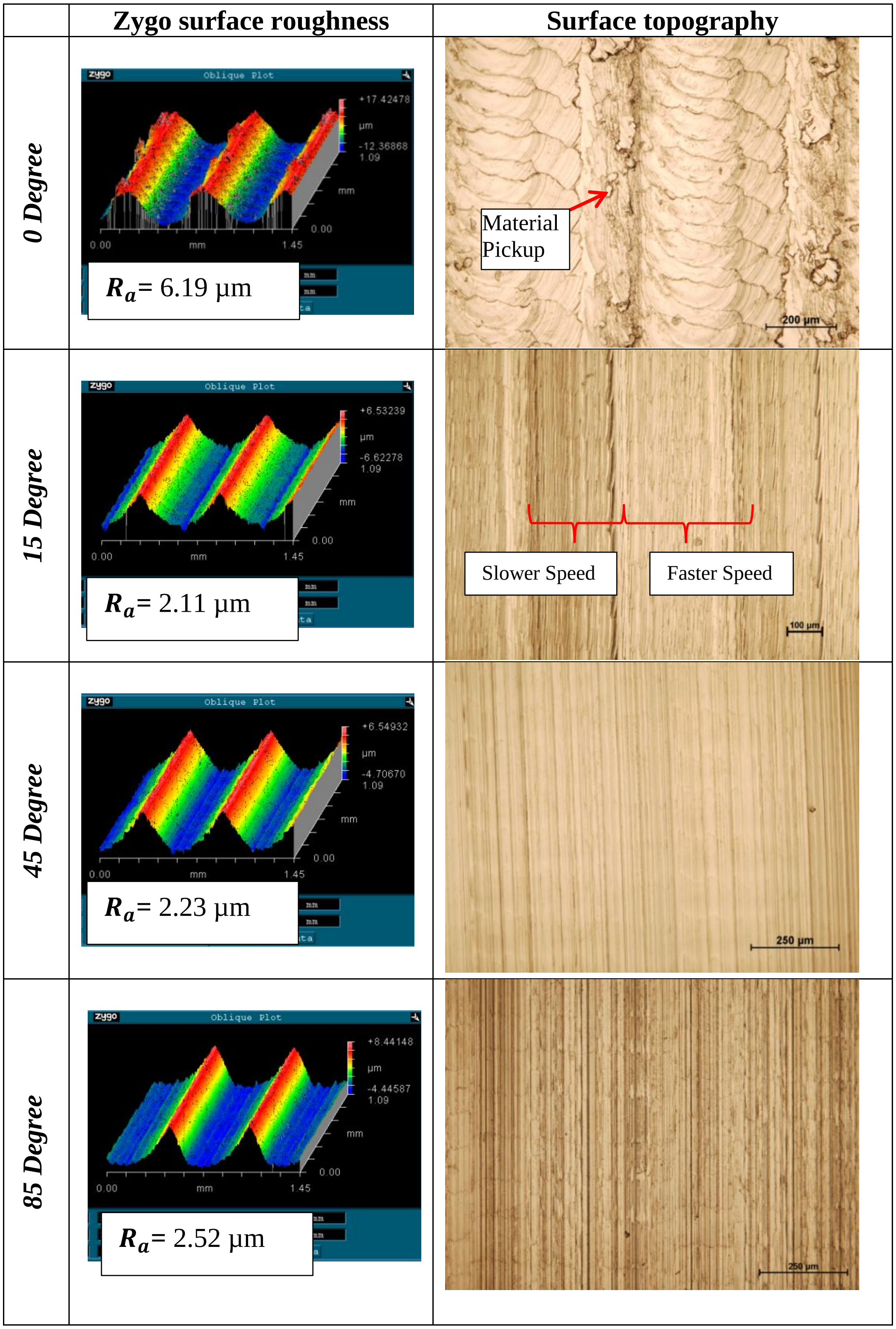

Figure 4-15: Surface roughness (R_a) with TiAlCrSiYN/TiAlCrN coated tool at different orientations.

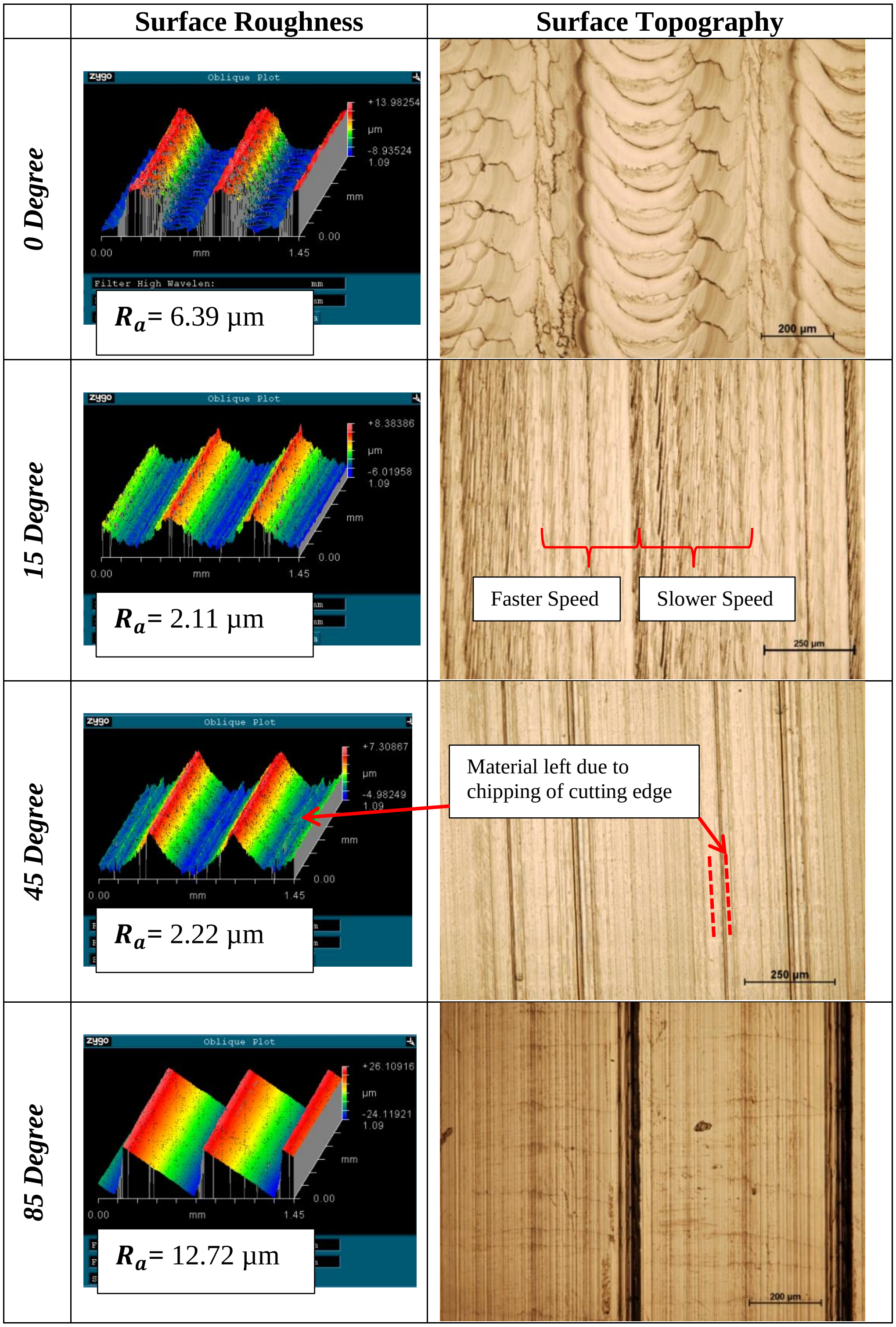

Figure 4-16: Surface roughness (R_a) with TiAlCrN coated tool at different orientation

4.3.2 Microstructure of machined surface

Figure 4-17 and Figure 4-18 illustrates the effect of machining with the TiAlCrSiYN/TiAlCrN and TiAlCrN coating tools on the workpiece microstructure at different tool orientations. Figure 4-17 illustrates that machining with the TiAlCrSiYN/TiAlCrN coating at 0 degrees (tip of the tool) causes 5µm of material flow layer along the machined surface. A similar material flow layer is observed for the remaining tool orientations. At 15 degrees, the depth of material flow decreased to approximately 2.5µm. At 45 degrees, the layer was further decreased to approximately 1.8µm, and finally at 85 degrees, no material flow layer was observed. Engaging the tool at different orientations mainly changes the cutting speed. At 0 degrees, where the cutting speed is slowest and the cutting speed range (ΔV) is highest, the depth of material flow is deepest. As the cutting speed increases and the cutting speed range (ΔV) decreases, the depth of material flow also decreases.

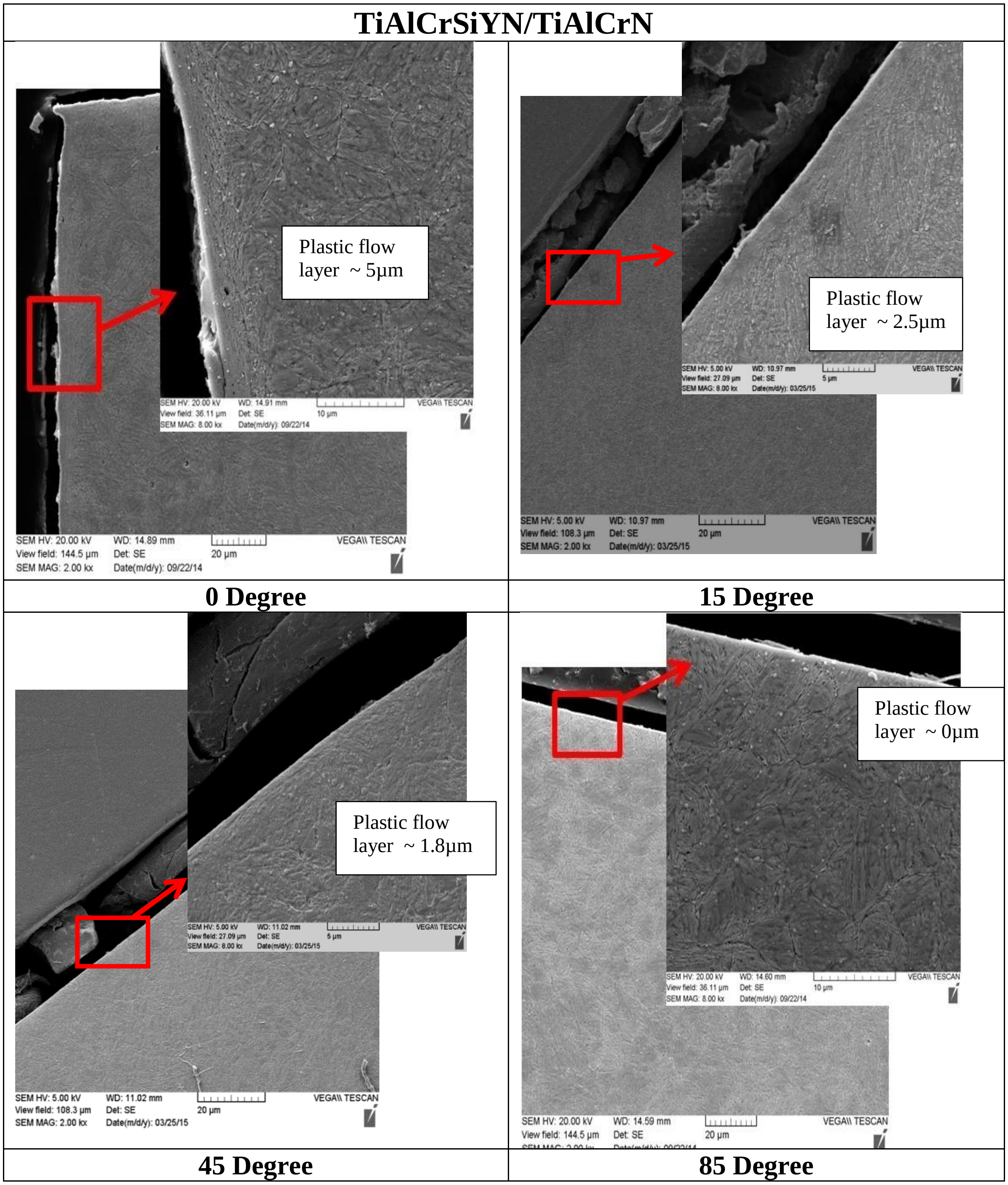

Figure 4-17: SEM of Microstructure of workpiece with TiAlCrSiYN/TiAlCrN coating at different orientations.

Figure 4-18 shows the microstructure of the workpiece with the TiAlCrN coated tool at different orientations. It was observed that a similar material flow layer exists as was earlier observed. At 0 degrees, 4 µm of material flow was observed. A similar trend was seen, that as the speed increased, the layer decreased such that at 15 degrees, 2.5 µm and at 45 degrees, a 1.75 µm flow layer was observed to be developed. The major difference was observed at 85 degrees where a 20 µm white layer was seen followed by a recrystallization zone. The reason being that the TiAlCrN tool at this stage had chipped as earlier seen in SEM images at the outer most radius which corresponds to 85 degree due to heavy load and high temperature thus exposing the carbide substrate and causing the workpiece material to experience plowing. At such a high speed, with the substrate exposed and coating destroyed, a significant amount of heat was generated. Some of this heat was conducted into the workpiece resulting in white layer formation and recrystallization.

In addition to speed, the instantaneous condition of cutting edge at the given location could also have an impact. It was earlier seen that the coating's oxidation is dependent on cutting condition and how changing the speed from 200 m/min to 500 m/min can alter the oxidation behaviour. At a different location along the cutting edge, the cutting speed varies, hence changing the wear mechanism. Also another challenge faced in ball nose end milling is the varying chip load along the helix angle. These factors change the wear mechanism along the cutting edge which can result in some significant changes in the microstructure.

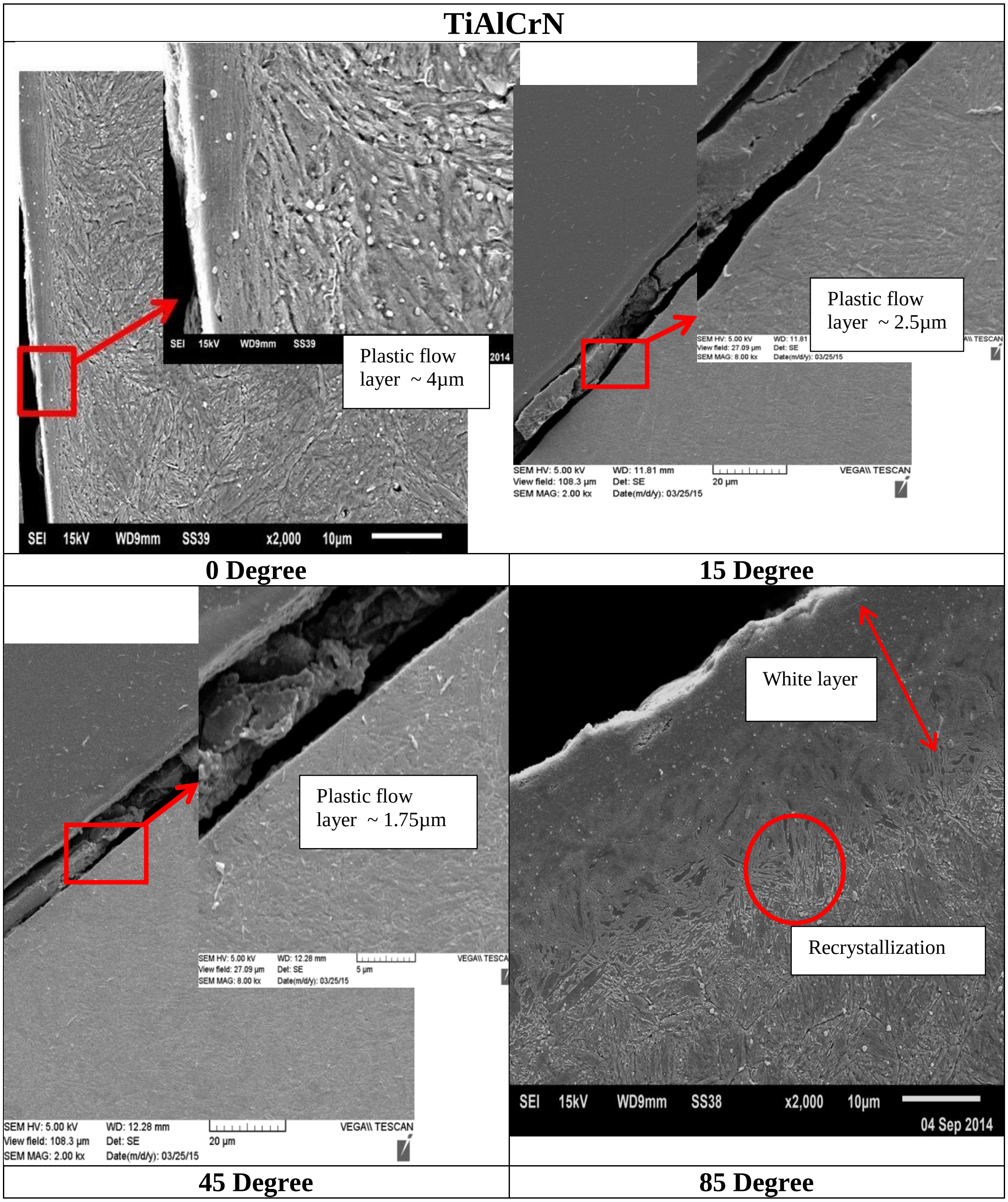

Figure 4-18: SEM of Microstructure of workpiece with TiAlCrN coating at different orientations.

4.3.3 Surface Residual Stress

The surface residual stresses developed in the hoop direction by both worn tools at different orientations are given in Table 4-3 and Table 4-4. Table 4-3 shows that at 0 degrees for TiAlCrSiYN/TiAlCrN the surface residual stress in the hoop direction was on the order of -276 MPa. At 15 and 45 degrees there was a slight decrease to -140MPa and -196 MPa. Finally at 85 degrees there was slight increase to -213MPa. As for TiAlCrN, a residual stress of -330Mpa was observed at 0 degrees, -430Mpa at 15 degrees, -155Mpa at 45 degrees and only -14MPa at 85 degrees. The decline of only -14MPa at 85 degrees is due to chipping of the TiAlCrN tool where the resulting rubbing motion generates heat, which shifts the residual stresses from compression towards tensile.

In all cases, compressive residual stresses were observed. In milling, the nature of cutting is interrupted; hence the workpiece experiences more mechanical work leaving high compressive residual stresses [Jawahir et al., 2011]. For the TiAlCrSiYN/TiAlCrN coating, high compressive residual stresses were observed. A comparison of the two coatings shows that the TiAlCrN coating gives relatively higher compressive residual stresses at 0 and 15 degrees, however at 45 and 85 degrees, the TiAlCrSiYN/TiAlCrN coated tool developed higher compressive residual stresses. This could be due to the different cutting behaviour of the two coatings operating under different conditions. Perhaps this is due to the different cutting speeds at each orientation. At slower cutting speeds, the TiAlCrN coating was able to provide better tribological conditions, whereas at higher speeds, the TiAlCrSiYN/TiAlCrN coating gave better performance. Cutting speed does alter the generated heat and its distribution. At higher speed more speed is generate of which get removed through the chips. At slower speed there is higher possibility of relatively more heat being conducted into the workpiece.

Table 4-3: Surface Residual stress of machined surface using TiAlCrSiYN/TiAlCrN coating

TiAlCrSiYN/TiAlCrN				
Residual Stress Hoop direction (MPa)	0 Degree	15 Degree	45 Degree	85 Degree
	-276 ± 26	-140 ± 8	-196 ± 14	-213 ± 13

Table 4-4: Surface Residual stress of machined surface using TiAlCrN coating

TiAlCrN				
Residual Stress Hoop direction (MPa)	0 Degree	15 Degree	45 Degree	85 Degree
	-330 ± 25	-430 ± 10	-155 ± 12	-14 ± 26

4.4 Attempts to Further Improve Tool life and Compatibility

Figure 4-19 illustrates the effect of Argon (Ar) etching time on the performance of the coating at 600m/min. Argon etching helps improve coating adhesion on the substrate of the tool. It is seen when the tool is etched for 5 minutes, the TiAlCrSiYN/TiAlCrN coating has a tool life of 133 m. Increasing the etching time to 7.5 minutes increases the tool life to 148 m of machining length. A further increase in etching to 10 minutes shows no improvement in tool life, with the tool still lasting 148 m. One of the requirements for the coating to be effective is its adhesion to the substrate material. By increasing the Ar etching time to 7.5 minutes, the surface is cleaner but after 7.5 minutes there is little improvement in observed tool life.

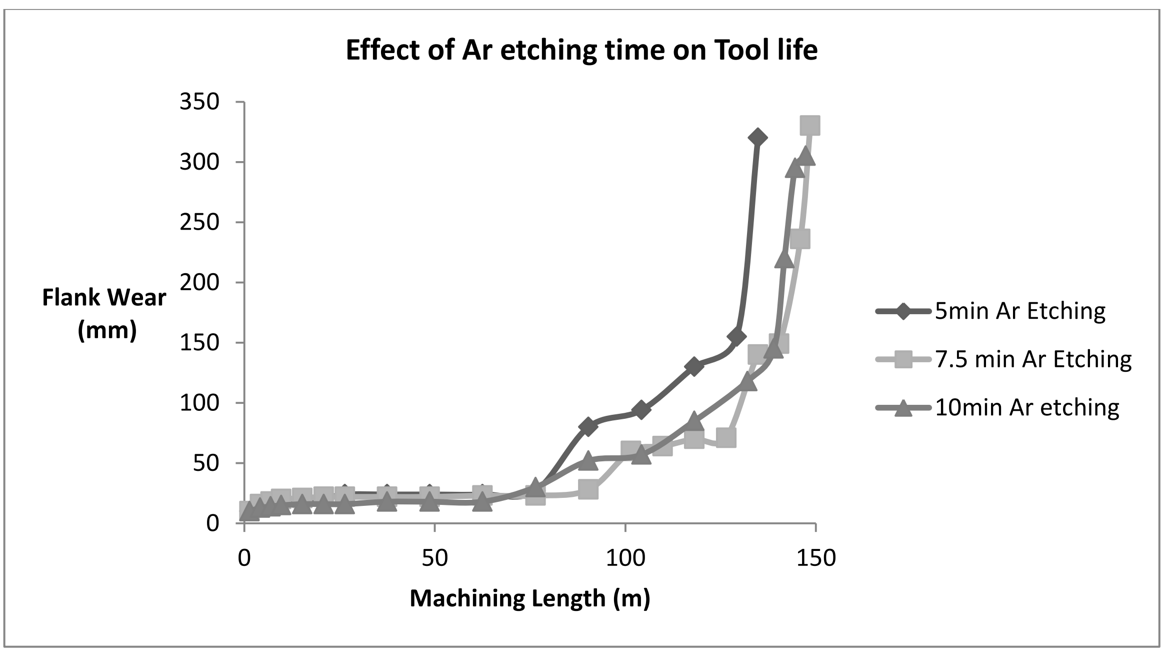

Figure 4-19: Effect of Ar etching time on life of TiAlCrSiYN/TiAlCrN coated tools at 600m/min.

It was earlier seen in section 4.1, the importance of various Tribo-oxide formations. Figure 4-20 shows attempts that were made to accelerate the generation of these oxides to further improve tool life. It is seen in Figure 4-20, at a cutting speed of 600m/min, (benchmark) the tool life was 148m. With a single burst of 700m/min (600_700x1), the tool life increased to 152m. With additional 700m/min passes resulting in a decrease of tool life as seen for 600_700x2 and 600_700x3 life which was measured to be 135.2m and 130m. At 700m/min the tool life further decreased to 85.6m. For adaptable coatings to perform, the wear should be minimal during the run in stage. Once the ‘self-organization' point is reached, it triggers the generation of tribo-oxides which allow for better protection and thus a more stable wear rate. The attempt here was to accelerate the tribo-oxide generation which could allow for a longer steady wear zone. In this test, the coating could not stand the harsh condition at 700 m/min even though they were short bursts, as shown in Figure 4-21. This test most likely caused initial damage to the coating and cutting edge which resulted in a decrease in tool life.

Though the tool was very carefully inspected under the microscope at early stages of its tool life to ensure there wasn’t chipping occurring, there could be a possibility of triggering rapid generation of rutile like oxide (TiO) which can play a role in the reduction of tool life. Moreover, the aspect of vibration wasn’t investigated here as it is also sensitive to RPM.

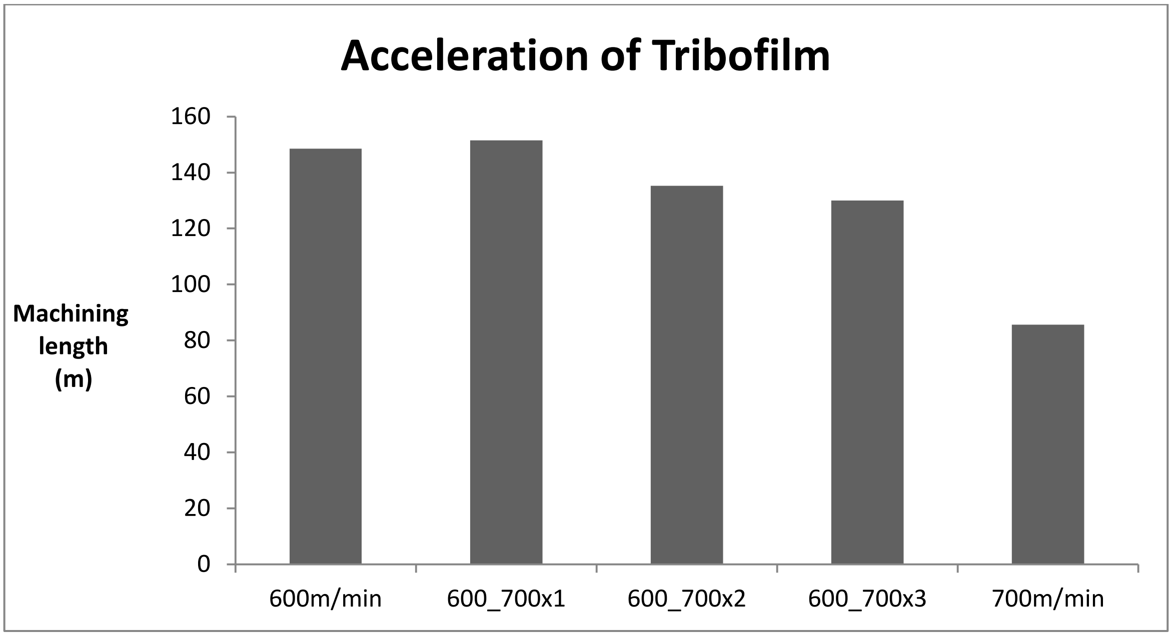

Figure 4-20: Attempt to Increase Tribo-oxide formation for TiAlCrSiYN/TiAlCrN coating

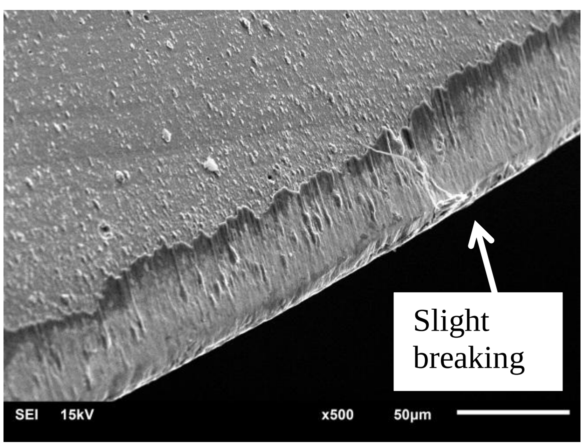

Figure 4-21: SEM image of TiAlCrSiYN/TiAlCrN coating after 1 pass at 700m/min

Chapter 5 Conclusion

This research can be broken down into four categories. Firstly, the effect of tool coatings on tool life was studied; how different alloying elements have an impact on coating performance. How these coatings form thin layers of oxides (Tribofilms) which play a crucial role in tool wear was illustrated. Secondly, how the cutting process changes with two different coated tools worn to a certain point was studied. Thirdly, the impact of tool wear on surface integrity at different tool orientations was studied. Finally, an attempt was made to accelerate the generation of these films by adjusting the initial cutting speed. Also the impact of argon etching time on tool life was also studied. The conclusion of this work was as follows:

In titanium based coating, the addition of alloying elements such as aluminum, Chromium, Silicon and Yttrium can greatly improve the performance of the tool. These elements improve the coating's mechanical and chemical properties by increasing hot hardness, resistance to oxidation, and minimizing grain growth at higher temperatures. In addition to alloying elements, structuring the coatings can greatly affect the performance as well. When comparing a monolayer coating with a multilayer coating, it is seen that the multilayer coating is preferred with the reasoning being that the multilayer coating can adapt better to wear by directing and controlling crack propagation.

The TiAlCrSiYN/TiAlCrN coating is characterized as a “Self-adaptive coating”. These coatings function by forming a thin layer of oxides which serve to protect the tool.

The particular alloying element present in the coating composition plays a crucial role in determining the type of oxide that forms on the coating surface. When comparing TiAlCrSiYN/TiAlCrN and TiAlCrN, different oxides on the tool surface were measured using XPS (Figure 4-5, Figure 4-6 and Table 4-1) and their contribution to tool wear was seen in the SEM images supplied (Figure 4-3 and Figure 4-4). For the TiAlCrSiYN/TiAlCrN coating, a higher level of protection was provided by the Aluminum and Chromium based oxide. In the case of the aluminum based oxides sapphire and mullite were found. These two compounds are extremely hard and possess excellent thermal barrier properties. In addition, the Chromium based oxide provided beneficial lubrication, resulting in reduced friction. There were also traces of Silicon based oxides which are also known to provide lubrication. The combination of these oxides resulted in minimal wear even after 100m of machining, as observed in SEM images of the tool wear zone. Characterization of TiAlCrN coatings illustrated an abundance of Ti based oxides. These oxides fail to provide protection at the higher operating temperatures experienced in this machining operation hence the severe wear observed in SEM images Figure 4-3 and Figure 4-4.

Chips formed from both TiAlCrSiYN/TiAlCrN and TiAlCrN coated tools after 100m were characterized. First, the underlay surface was observed using an SEM. It was seen that after 100m, the major mode of chip flow along the rake face was still sliding with very initial signs of sticking, however for TiAlCrN, the chip undersurface was wavy indicating the mode of chip flow to be "stick and slip". Also, the chips had torn edges which indicate plowing of the material. Next, the chip formation mechanism was compared for both coatings. For TiAlCrSiYN/TiAlCrN chips, the chip formation mechanism was saw tooth chips. The shear plane was well defined with a width of ~ 8μm. The Secondary shear deformation zone (SSDZ) had a width of ~ 2μm. For TiAlCrN chips, the chip formation mechanism was “continuous”. There was no defined shear plane and the SSDZ was comparatively wider (~ 6μm) due to the higher frictional force. Next the chip color from both coatings was compared as the tool was worn. For both tools the trend is similar; as the machining length increased, the tool wore and generated more heat, however after 100m, chips from the TiAlCrSiYN/TiAlCrN were “ green + blue + purple” indicating that the temperature in the cutting zone is >1000°C. Whereas for the TiAlCrN coated tool, the temperature was estimated to be >1100°C. Lastly, the micro-hardness of the chip’s cross section was compared. Both chips were softer near the SSDZ and harder at the bulk. Chips produced with the TiAlCrSiYN/TiAlCrN coated tool were comparatively softer. The reason behind this lies in how much thermal softening, strain hardening and quenching was involved.

Small blocks were machined to study the Surface integrity at different tool orientations using 100m worn TiAlCrSiYN/TiAlCrN and TiAlCrN coated tools. For each orientation, the cutting speed varied, therefore the cutting speed was calculated using CAM software as illustrated in Figure 4-12. The maximum cutting speed was at the 85 degree test and zero at the tip of the tool for the 0 degree test. Firstly the surface roughness and topography was compared. For both coatings at 0 degrees, the tool was smearing and plowing material giving a roughness of ~6μm. As the cutting speed increased, the surface roughness value decreased to ~ 2μm for both coatings. Surface roughness remained constant for TiAlCrSiYN/TiAlCrN since the tool wasn't as severely worn, even after 100m, however for TiAlCrN after the 45 degrees mark, the tool started to wear considerably. It can be seen in Figure 4-16, at 45 degrees the tool started to leave material on the part surface, and for 85 degrees where the tool had severely worn, the surface roughness was considerably higher, ~12µm. In addition, rather than machining scalloped shaped topography, at 85 degrees, the TiAlCrN tool machined steps, which is due to the width of chipping on the cutting tool. Next, the microstructure of the sublayer was analyzed. It was seen with TiAlCrSiYN/TiAlCrN at 0 degrees a material side flow layer of ~5µm was present on the part surface. This material side flow layer decreased as the cutting speed increased. A similar layer was observed for the TiAlCrN tool as well, however for 85 degrees, since the tool was worn exposing a carbide substrate, there was a higher level of heat being generated. This resulted in the formation of a white layer ~10µm, followed by a recrystallization layer. Lastly, the surface residual stresses in the cutting direction (hoop direction) was studied. It was seen that high compressive stresses were observed. At lower cutting speeds (0 and 15 degrees), relatively higher residual stresses were observed with TiAlCrN, and at higher cutting speeds (45 and 85 degree), the TiAlCrSiYN/TiAlCrN coated tool showed relatively higher residual stresses. This could be related to the oxidation property of the coating at the given cutting conditions. Perhaps the thermal barrier property of the oxide plays a role in changing the direction of heat flow along the cutting edge thus changing the residual stress profile.

It was established that TiAlCrSiYN/TiAlCrN performed better due to chemical composition and structure. Next, the coating parameter's influence on the performance of the coating was studied. Further, the effect of Ar etching time was studied. The increase of the Ar etching time from 5 minutes to 7.5 minutes resulted in a noticeable increase in tool life. However a further increase in Ar etching time showed no further improvement. The reason behind this improvement is that Ar etching helps clean the substrate surface which improves the adhesion of the coating.

Attempts were also made to accelerate tribofilm generation. One approach was to increase the cutting speed for a short burst at the start of cutting to increase heat without causing surface damage, however it was seen that a short burst was enough to damage the coating hence the accelerated testing failed to give a significant improvement in tool life.

Chapter 6 Future Work

1. It was established that Tribofilms play a major role in tool life which can have subsequent impact on surface integrity. Further alloying elements should be experimented with to better understand which can generate tribofilms that further enhance tool life and surface quality.
2. Since tribofilms are generated due to a sliding motion of the chip along the rake face, the effect of tool geometry of tribofilm generation should also be studied and optimized.
3. Vibration and dynamic studies should also be conducted to include their impact on tool life in assessing the overall performance of a tool.
4. Regarding surface integrity, material flow layers were observed. It would be interesting to study nano-mechanical properties of this layer. If they prove to be beneficial, then machining conditions can be adopted which can optimize their formation.

REFERENCES

Vyas, A. and Shaw, M.C. (1999), Mechanics of Saw-Tooth Chip Formation in Metal Cutting, ASME Journal of Manufacturing Science and Engineering, 121, 163–172.

Acchar, W., Gomes, U. U., Kaysser, W. A. & Goring, J. (1999), Strength degradation of a tungsten carbide-cobalt composite at elevated temperatures, *Materials Characterization, 43*(1), 27-32.

Armarego, E. J. A. & Brown, R. H. (1969), The machining of metals, *PRENTICE-HALL INC, ENGLEWOOD CLIFFS, N. J., 437P*

Astakhov, V.P. (2010), Surface Integrity – Definition and Importance in Functional Performance, In Davim, J. P. (Ed.), Surface Integrity in Machining (pp. 1-35). London: Springer London.

Axinte, D. & Dewes, R. (2002), Surface integrity of hot work tool steel after high speed milling-experimental data and empirical models, Journal of Materials Processing Technology, 127, 325–335.

Beake, B. D., Fox-Rabinovich, G. S., Losset, Y., Yamamoto, K., Agguire, M. H., Veldhuis, S. C., Endrino, J. and Kovalev, A.I. (2012), "Why can TiAlCrSiYN-based adaptive coatings deliver exceptional performance under extreme frictional conditions", *Faraday Discussions,*156(1), 267-277.

Bosheh, S.S. & Mativenga, P.T. (2006), White layer formation in hard turning of H13 tool steel at high cutting speeds using CBN tooling, International Journal of Machine Tools and Manufacture 46(2), 225−233.

Braghini Jr,A. & Coelho, R.T. (2001), An Investigation of the Wear Mechanisms of Poly crystalline Cubic Boron Nitride (PCBN) Tools when End Milling Hardened Steels at Low/Medium Cutting Speeds, International Journal of Advanced Manufacturing Technology 17,244-257.

Chen, L., El-Wardany, T. I., & Harris, W. C. (2004). Modelling the effects of flank wear land and chip formation on residual stresses, *CIRP Annals-Manufacturing Technology*, *53*(1), 95-98.

Cheng, K.(Ed.) (2008), *Machining dynamics: fundamentals, applications and practices*, London: Springer London

Chou, Y.K., Evans, C.J. (1999), White layers and thermal modelling of hard turned surfaces, International Journal of Machine Tools and Manufacture, 39, 1863–1881.

Dahlman, P. (2004), The influence of rake angle, cutting feed and cutting depth on residual stresses in hard turning, Journal of Materials Processing Technology, 147, 181–184.

Davim, J. P. (Ed.) (2010), *Surface integrity in machining* (Vol. 1848828742). London: Springer London

Ditmars, D., Ishihara, S., Chang, S., Bernstein, G., & West, E. (1982), Enthalpy and Heat-Capacity Standard Reference Material: Synthetic Sapphire (a-A1203) from 10 to 2250 K, Journal of research of the national bureau of standards, 87(2), 159

Donohue, L.A., Miinz, W.D., Lewis, D.B., Cawley, J., Hurkmans, T., Trinh, T., Petrov, I. and Greene, I.E., (1997), Large-scale fabrication of hard super-lattice thin films by combined steered arc evaporation and unbalanced magnetron sputtering, surface & Coaings Technology, 93 (1), 69-87.

Elbestawi, M.A., Srivastavi, A.K., El-Wardany, T.I. (1996), A model for chip formation during machining of hardened steel, Annals of the CIRP, 45(1), 71-76.

Electronica Machine tools Ltds. (2007) Electronicacarbide.com, Hard materials division, http://www.electronicacarbide.com.technical.html

Elfizy, A. (2008), Enhanced Conditions for High performance Machining of Hardened H13 Die Steel (Master’s thesis), McMaster University, Hamilton, ON.

El-Wardany, T.I., Kishawy, H.A. & Elbestawi, M.A. (2000), Surface integrity of die material in high speed hard machining, Part 2: Microhardness variations and residual stresses, J. Manuf. Sci. Eng. Trans. ASME 122(4), 632-641

Fallbbhmer, P., Altan, T., Tbnshoff, H.K., Nakagawa & T., Survay (1996), Survey of die and mold manufacturing industry, J. of Materials Processing Technology, 59, 158-168

Fallbbhmer, P., Rodriguez, C.A., Ozel, T. & Altan, T.(2000), High-speed machining of cast iron and alloy steels for die and mold manufacturing, J. of Materials Processing Technology, 98, 104-115.

Field, M. & Kahles, J.F. (1964), The surface integrity of machined and ground high strength steels, DMIC Report 210: 54–77.

Field, M., Kahles, J.F. & Cammett, J.T. (1972), Review of measuring methods for surface integrity, Annals of the CIRP, 21, 219–238.

Finch, G.I., Quarrell, A. G. & Roebuck, J. S. (1934), The Beilby Layer. Proceedings of the Royal Society of London, Series A 145(855): 676−681.

Fox-Rabinovich, G. & Totten, G. (ed) (2006), Self-Organization During Friction: Advance Surface Engineered Materials and Systems Design (Boca Raton, FL: CRC Press)

Fox-Rabinovich, G., Kovalev, A., Veldhuis, S., Yamamoto, K., Endrino, J. L., Gershman, I. S ., Rashkovskiy, w., Aguirre, M., & Wainstein, D. L. (2015), Spatio-temporal behaviour of atomic-scale tribo-ceramic films in adaptive surface engineered nano-materials, Scientific reports 5.

Fox-Rabinovich, G.S., Wilkinson, D.S., Veldhuis, S.C., Dosbaeva, G.K., Weatherly, G.C. (2006), Oxidation resistant Ti-Al-Cr alloy for protective coating applications, Intermetallics 14, 189-197.

Fox-Rabinovich, G.S., Yamamoto, K., Veldhuis, S.C., Kovalev, A.I., Shuster L.S. and Ning, L. (2006), Self-adaptive wear behaviour of nano-multilayered TiAlCrN/WN coatings under severe machining conditions, Surface and Coatings Technology 201(3-4), 1852-1860.

Fox-Rabinovich, G.S., Yamomoto, K., Veldhuis, S.C., Kovalev, A.I., Dosbaeva, G.K., (2005), Tribological adaptability of TiAlCrN PVD coatings under high performance dry machining conditions, Surface & Coatings Technology 200, 1804-1813.

Fox-Rabinovich ,G. S., Yamamoto, K., Beake, B. D., Gershman, I. S., Kovalev, A. I., Veldhuis, S. C., Aguirre, M. H., Dosbaeva, G. and Endrino, j. L.(2012). Hierarchical adaptive nanostructured PVD coatings for extreme tribological applications: the quest for nonequilibrium states and emergent behaviour. Science and Technology of Advanced Materials. 13(4), 043001.

Fox-Rabinovich,G.S., Yamomoto, K., Veldhuis, S.C., Kovalev, A.I., Dosbaeva, G.K. (2005). Tribological adaptability of TiAlCrN PVD coating under high performance dry machining condition, Surface & Coating Technology 200, 1804-1813.

G. S. Fox-Rabinovich, B. D. Beake, K. Yamamoto, M. H. Aguirre, S. C. Veldhuis, G. Dosbaeva and L. S. Shuster, (2010), "Structure, properties and wear performance of nano-multilayered TiAlCrSiYN/TiAlCrN coatings during machining of Ni-based aerospace superalloys," *Surface and Coatings Technology,* vol. 204, no. 21, 3698-3706.

Griffiths, B.J. (1993) Modeling complex force system, Part 1: The cutting and pad forces in deep drilling. ASME Transactions, Journal of Engineering for Industry 115: 169-176.

Grzesik W (2008) Advanced Machining Processes of Metallic Materials, Elsevier, Amsterdam.

Grzesik, W.& Nieslony, P. (2003), Thermophysical property based selection of tool protective coatings for dry machining of steels, Journal of Manufacturing Science and Engineering, Transactions of the ASME 125(4), 689-695.

Grzesik, W., Kruszynski, B., Ruszaj A., (2010).Surface Integrity of Machined Surface. In Davim, J. P. (Ed.), Surface Integrity in Machining (pp. 143-179). London: Springer London.

Hirao, M., Terashima, A., Joo, H.Y., Shirase, K. & Yasui, T.(1998), Behavior of cutting heat in high speed cutting, J. Jpn, Soc. Precision Eng., 64(7), 1067-1071.

Holleck, H. & Schier, V., (1995), Multilayer PVD coatings for wear protection, Surface and Coating Technology 76-77, 328-336.

Hudson, B. (1992) Surface Science − An Introduction, Boston: Butterworth-Heine- mann.

Hynes, A. P. & Doremus, R. H. (1991), High Temperature Compressive Creep of Polycrystalline Mullite, J. Am. Ceram. Soc, 74, 2469–2475

ISO 4287:1997. Written standard – Image Metrology

ISO 4288:1996. Geometrical Product Specification (GPS) – Surface Texture: Profile method-Rules and procedures for the assessment of surface texture.

Jawahir, I. S., Brinksmeier, E., M'Saoubi, R., Aspinwall, D. K., Outeiro, J. C., Meyer, D., ... & Jayal, A. D. (2011). Surface integrity in material removal processes: Recent advances. *CIRP Annals-Manufacturing Technology*, *60*(2), 603-626.

Kaczmarek, J. (1976), Principles of Machining by Cutting, Abrasion and Erosion, Peter Peregrinus Limited, Stevenage.

Klocke, F. & Kratz, H. (2005), Advanced tool edge geometry for high precision hard turning, Annals of the CIRP, 54(1), 47−50.

König, W., Klinger, M., & Link, R. (1990), Machining hard materials with geometrically defined cutting edges—field of applications and limitations. CIRP Annals-Manufacturing Technology, 3(1), 61–64.

Kopac, J., Sokovic, M. & Dolinsek, S.,(2001), Tribology of coated tools in conventional and HSC machining, Journal of Materials Processing Technology ,118(1-3), 377-384.

Kukla, R., (1997). Magnetron Sputtering on large scale substrate: an overview on the state of the art, Surface and Coatings Technology, 93(1), 1-6.

Lanin, A. G., Muravin, E. L., Popov, V. P., & Turchin, V. N. (2003), Thermal shock resistance and thermal-mechanical processing of sapphire, *Journal of the European Ceramic Society*, *23*(3), 455-468

Lewis, D.B., Donohue, L.A. Lembke, M. Munz, W.D. Kuzel, R. Valvoda, V., Blomfield, C.J. (1999), The influence of the yttrium content on the structure and properties of

Tii.x.y.zAlxCryYzN PVD hard coatings, Surface & Coatings Technology 114(2-3), 187-199.

Li, W., Guo, Y., & Guo, C. (2013), Superior surface integrity by sustainable dry hard milling and impact on fatigue, CIRP Annals - Manufacturing Technology, 62(1), 567–570.

Löffler, F. H. (1994), Systematic approach to improve the performance of PVD coatings for tool applications, *Surface and Coatings Technology*, *68*, 729-74

Elbestawi, M. A., Srivastava, A. K., & El-Wardany, T. I. (1996). A model for chip formation during machining of hardened steel. *CIRP Annals-Manufacturing Technology*, *45*(1), 71-762

Shaw, M.C., Vayes, A. (1993), Chip Formation in the Machining. Annals of CIRP, 42(1), 29–33.

M'Saoubi, R., Outeiro, J.C., Chandrasekaran, H., Dillon Jr., O.W. and Jawahir, I.S. (2008) A review of surface integrity in machining and its impact on functional performance and life of machined products. Int. J. Sustainable Manufacturing 1(1/2): 203−236

Movahhedy, M. R., Altintas, Y., & Gadala, M. S. (2002), Numerical analysis of metal cutting with chamfered and blunt tools, *Journal of Manufacturing Science and Engineering*, *124*(2), 178-188

Ning, L. (2007). Nano-multilayered Self-adaptive Hard PVD Coatings for Dry High Performance Machining (Doctoral dissertation). McMaster University, Hamilton, ON.

Ning, Y., Rahman, M., Wong, Y.S.(2001), Investigation of chip formation in high speed end milling, Journal of Material Processing Technology 113, 360-367.

PalDey, S. & Deevi, S.C.(2003). Properties of single layer and gradient (Ti,Al)N coatings, Material Science and Engineering A 361(1-2),1-8.

PalDey, S. & Deevi, S.C.(2003). Single layer and multilayer wear resistant coating of (Ti,Al)N: a review, Material Science & Engineering A 342, 58-79.

Petropoulos, G.P., Pandazaras, C.N., Davim, J. P., (2010). Surface Texture Characterization and Evaluation Related to Machining. In Davim, J. P. (Ed.), Surface Integrity in Machining (pp. 37-66). London: Springer London.

Recht, R. F. (1985). A Dynamic Analysis of High-Speed Machining. Journal of Engineering for Industry, 107(4), 309.

Ren, H., & Altintas, Y. (2000), Mechanics of machining with chamfered tools, *Journal of manufacturing science and engineering*, *122*(4), 650-659

Roberts, G. A., Kennedy, R., & Krauss, G. (1998), *Tool steels*. ASM international

Scheel J and Fukuda T (ed) (2003), Crystal Growth Technology (New York:Wiley)

Schulz B, 1988, J. Nucl. Mater. 155–157, 348.

Schulz, H., Moriwaki, T.(1992), High-speed machining, Annals of the CIRP, 41(2), 637-643.

Shaw, M.C. & Vyas, A. (1993), Chip formation in the machining of hardened steel, Annals of CIRP, 42(1), 29-33.

Smith, I.J., Gillibrand, D., Brooks, J.S., Münz, W.-D., Harvey, S. and Goodwin, R., (1997), Dry cutting performance of HSS drills coated with improved TiAlN, Surface and Coating Technology, 90(1-2), 164-171.

Sreejith, P. S., & Ngoi, B. K. A. (2000). Dry machining: machining of the future, *Journal of materials processing technology*, *101*(1), 287-291

Srivastava, A., Joshi, V. & Shivpuri, R. (2004), Computer modeling and prediction of thermal fatigue cracking in die-casting tooling, Wear, 256(1-2), 38–43.

Stachowiak, G., & Batchelor, A. W. (2013). *Engineering tribology*. Butterworth-Heinemann

Stead, J.W. (1912), Micro-metallography and its practical applications, Journal of West- ern Scottish Iron and Steel Institute 19, 169–204.

Stephenson, D. A. & Agapiou, J. S.(1997), Metal Cutting Theory and Practice, *New York*

Suzuki, T., Huang, D. and Ikuhara, Y. (1998). Microstructures and grain boundaries of (Ti,Al)N films, Surface and coating technology ,107, 41- 47.

Tlusty, J. & Masood, Z. (1978), Chipping and breakage of carbide tools, *Journal of Manufacturing Science and Engineering*, *100*(4), 403-412.

Tlusty, J. (1993), High-speed machining, Annals of the CIRP, 42 (2), 733-738.

Tönshoff, H., Arendt, C., & Amor, R. (2000), Cutting of hardened steel, CIRP Annals-Manufacturing Technology, 49, 547–566.

Tönshoff, H.K., Denkena, B., Friemuth, T., Spengler, C. (2002), influence of different grinding processes on coating adhesion on cutting tools, Proceedings of the 3rd International Conference – The Coating in Manufacturing Engineering and EUREKA Partnering Event, 3-16.

Yamamoto, K., Kujime, S. and Takahara, K. (2005), Properties of nano-multilayer hard coatings deposited by a new hybrid coating process: Combined cathodic arc and unbalanced magnetron sputtering, Surface and Coating Technology, 200(1-4), 435-439.

Yen, Y. C., Söhner, J., Weule, H., Schmidt, J., & Altan, T. (2002). Estimation of tool wear of carbide tool in orthogonal cutting using FEM simulation.*machining science and technology*, *6*(3), 467-486

Zhang, S., Ding, T., & Li, J. (2012), Determination of surface and in-depth residual stress distributions induced by hard milling of H13 steel, Production Engineering, 6(4-5), 375–383.

Zhang, S., Sun, D., Fu, Y. & Du, H. (2003), Recent advances of superhard nano-composite coatings: a review, Surface & Coatings Technology, 167, 113-119.